2016

Inverse Turbulence Modeling of channel flow using Continuous Adjoint method

Kumar Vishal
Iowa State University

Inverse turbulence modeling of channel flow using continuous adjoint method

by

Kumar Vishal

A thesis submitted to the graduate faculty

in partial fulfillment of the requirements for the degree of

MASTER OF SCIENCE

Major: Aerospace Engineering

Program of Study Committee:

Paul A. Durbin, Major Professor

Leifur Leifsson

Ran Dai

Iowa State University

Ames, Iowa

2016

DEDICATION

To my father, Paras Nath Rai, & my mother, Dharmsheela Rai.

TABLE OF CONTENTS

LIST OF TABLES

LIST OF FIGURES

ACKNOWLEDGEMENTS

I would like to express my deepest thanks to Professor Paul Durbin for his patience and guidance during the course of this project. His way of looking at scientific problems will always be a source of inspiration to me.

My sincere thanks to Professor Leifur Leifsson and Professor Ran Dai for kindly serving on my graduate committee. Special thanks to Professor Karthik Duraisamy for helping me with the technical aspects of inverse design implementation.

Thanks to Mr. Andrew Thelen for helping me out with various aspects of MATLAB optimization techniques. Lastly, I would also like to express my gratefulness to my research colleagues, Mr. Zifei Yin, Mr. Rikhi Bose, Mr. Umair Ismail, Mr. Racheet Matai & Mr. Rajarshi Biswas for their help and discussions which made this work fun and enjoyable.

ABSTRACT

In this thesis, a formal approach for inferring the functional forms of information that might be missing in Wilcox's $k-\omega$ model for turbulent channel flow has been presented. Different terms of $k-\omega$ transport equations have been *modified* by including a *spatial* parameter. The resulting inverse problem has been efficiently solved using *continuous* adjoint method to accurately predict mean velocity. In many cases, a simplifying assumption of a "frozen" eddy viscosity in the turbulence model has been made to arrive at the final set of adjoint equations. Good agreement between inferred solution and corresponding DNS data has been demonstrated, first, for plane channel flow and later, for channel flow with spanwise rotation where *re-laminarization* of fluid takes place. Finally, some parameters have been explored that seem to scale the corrections.

CHAPTER 1. INTRODUCTION

1.1 Background

1.1.1 The turbulence problem

Turbulent flows are complex, multiscale phenomenon of utmost practical importance [12]. The Navier-Stokes (NS) equations [1.1] govern the physics of all viscous, incompressible fluid flows, whether laminar or turbulent. Theoretically, NS equations are quite deterministic; this means that if proper initial and boundary conditions are specified, equation 1.1 can be used to determine the evolution of dependent variables completely. However, the non-linearity (advection term) of equation 1.1 makes it highly sensitive; such that many realizations are possible for infinitesimal difference in flow conditions [7]. Turbulent flows, unlike laminar flows, have the additional complexity that they are multi-scale phenomenon. This means that motions in turbulent flows happens across a bandwidth of scales from large scales determined by the geometry to small scales determined by molecular viscosity [11]. Generally, theoretical solutions of NS equations for turbulent flows don't exist; so, it's imperative to study them numerically.

$$\begin{aligned} \frac{\partial u_i}{\partial x_i} &= 0 \\ \frac{\partial u_i}{\partial t} + u_j \frac{\partial u_i}{\partial x_j} &= -\frac{1}{\rho}\frac{\partial p}{\partial x_i} + \nu \frac{\partial^2 u_i}{\partial {x_j}^2} \end{aligned} \tag{1.1}$$

The growth in computing power has made high-fidelity numerical simulations of various turbulent flow configurations possible. Direct Numerical Simulation (DNS) and Large Eddy Simulation (LES) have been able to solve problems with greater accuracy and speed. However, due to their speed and memory requirements, the implementation of DNS & LES has been limited to simple flow configurations and low Reynolds numbers only. To resolve all the scales in turbulent motion, equations 1.1 must be discretized with very large number of computational

points, which increases with increasing Reynolds number. Solving full Navier-Stokes equations numerically, for practical turbulent flows for realistic Reynolds numbers, remains infeasible in near future [28].

1.1.2 Statistical approach towards turbulence

One way to circumvent the problem of solving the full NS equations is by studying turbulent flows statistically. Most practical applications require information, like skin friction or pressure coefficient, that depend on statistics of the flow; hence, studying turbulent flows statistically makes sense. One way of doing this is by using Reynolds decomposition, wherein a random field ϕ is decomposed into its mean $\left(\bar{\phi}\right)$ and fluctuating component(ϕ') as:

$$\phi = \bar{\phi} + \phi' \tag{1.2}$$

Substituting such decomposition for velocity and pressure fields in 1.1 and averaging over time yields the famous Reynold's Averaged Navier-Stokes (RANS) equations [1.3]. RANS equations are similar to NS equations except for the last term having $\overline{u_i' u_j'}$, called *Reynold stresses*, which is a direct consequence of having non-linearity in the system.

$$\begin{aligned} &\frac{\partial \bar{u}_i}{\partial x_i} = 0 \\ &\frac{\partial \bar{u}_i}{\partial t} + \bar{u}_j \frac{\partial \bar{u}_i}{\partial x_j} = -\frac{1}{\rho}\frac{\partial \bar{p}}{\partial x_i} + \nu \frac{\partial^2 \bar{u}_i}{\partial {x_j}^2} - \frac{\partial}{\partial x_j}\left(\overline{u_i' u_j'}\right) \end{aligned} \tag{1.3}$$

Solving equation 1.3 requires the determination of Reynold stresses wherein lies the problem of studying turbulence statistically.

1.1.3 The closure problem of turbulence

Taking a statistical approach towards turbulence shifts the strategy from solving a perfectly deterministic problem (NS) to solving a problem which is not deterministic (RANS) any more [7]. The RANS equations are *unclosed* set of equations; in the sense that there are more variables than equations. Specifically, there are 4 equations (1 continuity & 3 momentum) in 10 unknowns (1 pressure, 3 velocity components & 6 components of stress tensor, $\overline{u_i' u_j'}$), for

a 3-D case. Any efforts to close the system by obtaining an equation for $\overline{u_i' u_j'}$ from 1.1 results in an equation with $\overline{u_i' u_j' u_k'}$ and so on [7]. In order to make this system deterministic again, "additional" information is required form the outside.

1.1.4 Turbulence modeling

Turbulence Modeling deals with predicting, both qualitatively and quantitatively, the effects of turbulence on mean flow and vice versa by using a model to evaluate Reynolds stresses. The usefulness of turbulence modeling is that it provides the "additional" information required to close 1.3 at a very low computational cost when compared to LES or DNS.

One of the consequences of presence of turbulence is an enhanced rate of momentum transfer in the fluid flow. Most RANS turbulence models used today are based on an assumption, called *Boussinesq* assumption, that the momentum transfer due to turbulent motion can be modelled using an extra viscosity, called eddy viscosity, acting on the laminar fluid flow [6]. This is analogous to the idea that the momentum transfer due to molecular motion of the fluid can be modelled using the molecular viscosity of the fluid. The eddy viscosity can be obtained by solving either an algebraic equation, for example in mixing length models, or by solving some additional transport equations (represented in equation 1.4 for a quantity x) as in scalar eddy-viscosity models.

$$\begin{aligned} &\frac{Dx}{Dt} = P_x - D_x + Di_x \\ &\text{where,} \\ &P_x \rightarrow \text{Production of x} \\ &D_x \rightarrow \text{Destruction of x} \\ &Di_x \rightarrow \text{Diffusion of x} \end{aligned} \tag{1.4}$$

Scalar eddy viscosity turbulence models, particularly the k-ϵ & k-ω variations[38], are immensely popular for most industrial applications. In this work Wilcox's k-ω model has been used for all the calculations.

In other more complex turbulence models, such as the Reynolds stress and the PDF mod-

els, eddy viscosity assumption has been discarded completely and the Reynolds stresses are evaluated directly [30].

1.1.5 Inverse modeling

Inverse modeling or inverse design involves finding of the *question* that yields a particular solution rather than the other way around [22]. It necessitates *minimization* of a function (called *objective* or *cost* function) subjected to a set of constraints. One of the major tasks in inversion is the calculation of gradient of the objective function with respect to *design* variables. Calculating gradient directly becomes expensive if dimension of the *design* variable is large. Usefulness of Adjoint method is in that it makes gradient calculation computationally cheap; equivalent to solving one more flow equation[16]. There are two major classifications of adjoint methods, discrete and the continuous, with various studies dedicated to device a hybrid approach as well [36, 35]. While the former strategy obtains the *discrete* form of adjoint equations directly from flow equations, in the latter, first a *continuous* set of adjoint equations are obtained which are discretized later. This study follows the work of Parish and Duraisamy [26] to lay the basic framework of inversion using the *continuous* adjoint approach.

1.2 Motivation

RANS turbulence models typically produce good results for simple flow configurations. But, as the flow becomes complex, which is the case with most flows of any practical importance whatsoever, their limitations become apparent. For example, modeling flows experiencing separation, adverse pressure gradients or streamline curvature/rotation is especially difficult with scalar eddy viscosity turbulence models[31],[39].

Flows with streamline curvature/rotation have great practical relevance, for example, in turbo machinery. Turbulence can get suppressed or enhanced by the presence of centrifugal force, which comes into play due to curvature/rotation effects. Rotation doesn't directly affect the kinetic energy of the mean flow, instead it creates anisotropy which alters the production of turbulent energy, which, in turn, affects the mean flow [10]. Since the effect of rotation is *direction* dependent, eddy viscosity turbulence models, by design, are insensitive to system

rotation/curvature. It is highly likely, however, that RANS modeling will remain the primary tool for simulating turbulent flows, even the complex ones, in the coming decade [28]. Therefore, a lot can be gained by improving the predicting capabilities of these models for flows with curvature/rotation.

The failure of eddy viscosity models, sometimes, is attributed to the simplicity of classical turbulence modeling approach [37]. The framework of these models are build on the knowledge of flow physics. They also contain a set of tunable coefficients which are calibrated using a small number of simple test cases. When such basic models are applied to complex flows, the coefficients have to be recalibrated. However, even after recalibration, the models are not universal and their accuracy is diminished if the flow conditions are altered. One of the criticisms of this approach is that while it is data driven to an extent, in the sense that the coefficients are sometimes adjusted based on experimental and numerical findings, it doesn't include a formal *strategy* to inform model development process [9].

1.3 Literature Review

A great amount of research effort has gone into sensitizing the k-ω turbulence model and its variants for curvature/rotation effects. Methods to sensitize the scalar eddy viscosity models can be categorized either into a *Modified Coefficients* approach or a *Bifurcation* approach. A detailed machinery used in the two mentioned approaches can be found in [10]. Since this study follows a methodology analogous to modified coefficients approach, a brief review has been provided in the following paragraphs.

In Modified coefficients approach, the model coefficients are tuned such that the production of turbulent kinetic energy is either suppressed or enhanced [2]. Spalart and Shur (1997)[34] modified the production term of eddy viscosity transport equation, by giving it parametric dependence on the inner product between vorticity and rotation vectors, to sensitize it for system rotation. Hellsten [18] provided some modifications to the Menter's k-ω SST model by introducing an additional, rotation sensitive, parameter in destruction term of ω-equation. Results were found to be encouraging, but were limited to very small rotation numbers ($Ro <$ 0.1) only. Smirnov and Menter [33] extended the Spalart-Shur correction into k-ω SST model

by correcting the production terms of both, k & ω equations. More recently, Arolla and Durbin [3] proposed a modification to the production term of ω-equation.

Application of inverse design in CFD is not new. Most of the initial efforts in this direction were primarily in the context of aerodynamic *shape design*. Pironneau [29] first applied the ideas of optimal control theory to fluid dynamics problems. Jameson (1988) posed the problem of finding the "optimal" shape of an aerodynamic body, subject to a set of constraints, as an inverse problem. In 1980s and 90s, Jameson used adjoints to handle Euler equations[19] and Navier-Stokes equations[21]. The application of inverse design was further extended to RANS equations by Zymaris et al. [41] & Dow and Wang [8].

Most of the previous work in utilizing inverse design in turbulence modeling has been focused mainly towards quantifying uncertainties in model coefficients [5, 25, 8]. In an effort to extend this work to *reconstruct functional* fields, Duraisamy *et al.* have laid out a formal strategy to use high-fidelity data to inform closure modeling. This strategy basically consists of three steps. First, the problem is set up as an *inverse problem* to extract the *funcional* form of deficiencies. Many sample test cases have been dealt with in references [26, 9]. This step on its own, they argue, can provide valuable modeling insight. In the second step, *machine learning* strategies is used to reconstruct the missing *functional* information [37], and the last step consists of injecting the corrections in the turbulence models for improved predictions [40, 27, 32].

In lieu of the above discussions, the particular focus of this work is to set up the turbulent channel flow problem for *inversion* to extract the *missing* information. This closely follows step 1 of the *strategy* outlined by Duraisamy *et al.*. *Continuous* adjoint approach, instead of the *discrete* aproach used by Parish and Duraisamy [26], has been used to calculate the gradients. Inversion has first been performed for non-rotating channel flow using the DNS data of Moser et al. [24]. Then the approach has been extended to rotating channel flow cases of Kristoffersen and Andersson [23] & Grundestam et al. [17] based on Rotation number, Ro_b. Finally, some *scaling* parameters, as identified by Parish and Duraisamy [26], have been explored as an extension of the current work.

CHAPTER 2. THEORETICAL FORMULATION

2.1 Problem Description

A turbulent flow between two plane parallel (fixed) plates separated by a distance $2h$ has been considered [figure 2.1a]. The mean velocity is primarily in the x-direction, also called the streamwise direction. The y & z directions are called the wall-normal and spanwise directions respectively. Under the assumption that the channel is large in stream-wise and spanwise directions, to mitigate wall effects and study *fully-developed* region only, the flow becomes homogeneous in x & z. Flow is also assumed to have reached steady state.

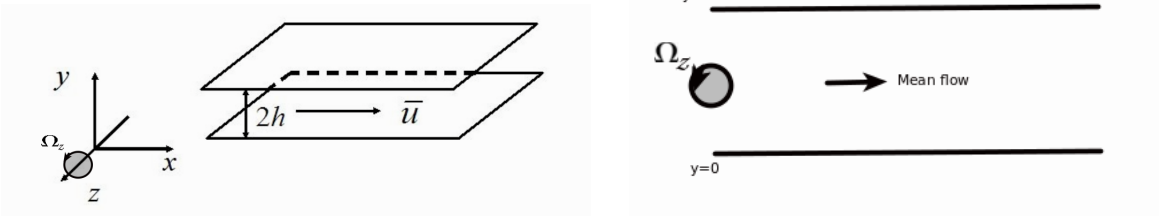

(a) Flow between two parallel plates (from ref. [15])

(b) A 2D equivalent

Figure 2.1: Channel flow with spanwise rotation

A steady, homogeneous channel flow can be considered a quasi one dimensional flow as depicted in figure 2.1b , where velocity statistics depend only on y coordinate. Both rotating and non-rotating channel flows have been considered for this study. A constant rate of rotation, $\vec{\Omega} = \Omega_j = (0, 0, \Omega_z)$, has been applied for rotating case.

2.2 Governing Equations

2.2.1 Introduction

Since studying channel with spanwise rotation has been the primary focus of this study, statistical governing equations for rotating channel have been discussed in the following sections. Equations for non-rotating channel can be obtained simply by dropping Ω_z terms.

2.2.2 Discussion on RANS

With the introduction of rotation, centrifugal and Coriolis forces have to be accounted for in original NS equations [1.1]. The contribution from centrifugal force $\left(\vec{\Omega} \times \left(\vec{\Omega} \times \vec{r}\right)\right)$ gets absorbed in the pressure term to yield a modified pressure distribution, P_{eff}. Equations 2.1 is the final form of Navier-Stokes for channel with spanwise rotation. The last term in 2.1 is a direct contribution from Coriolis forces $\left(2\vec{\Omega} \times \vec{u}\right)$.

$$\begin{aligned} &\frac{\partial u_i}{\partial t} + u_j \frac{\partial u_i}{\partial x_j} = -\frac{1}{\rho}\frac{\partial P_{eff}}{\partial x_i} + \nu \frac{\partial^2 u_i}{\partial x_j^2} - 2\epsilon_{ijk}\Omega_j u_k \\ &\text{where,} \\ &P_{eff} = p + \frac{\Omega_z^2 r^2}{2} \qquad \& \qquad r^2 = x^2 + y^2 \end{aligned} \tag{2.1}$$

Decomposing $u_i\,(= \bar{u}_i + u_i')$, averaging 2.1 and noting that $\frac{\partial \bar{u}_j}{\partial x_j} = 0$ yields RANS equations (2.2) for a system with spanwise rotation.

$$\frac{\bar{D}\bar{u}_i}{\bar{D}t} = -\frac{1}{\rho}\frac{\partial \bar{P}_{eff}}{\partial x_i} + \frac{\partial}{\partial x_j}\left[\nu\left(\frac{\partial \bar{u}_i}{\partial x_j} + \frac{\partial \bar{u}_j}{\partial x_i}\right) - \overline{u_i' u_j'}\right] - 2\epsilon_{ijk}\Omega_j \bar{u}_k \tag{2.2}$$

Since the flow considered to be homogeneous in x & z, the continuity equation gets reduced to $\frac{\partial \bar{v}}{\partial y} = 0$. Hence, the x, y & z momentum equations can be written as,

$$\begin{aligned} x - eq^n \quad &: \quad \frac{\partial}{\partial y}\left(\nu\frac{\partial \bar{u}}{\partial y} - \overline{u'v'}\right) = -\frac{1}{\rho}\frac{\partial \bar{P}_{eff}}{\partial x} \\ y - eq^n \quad &: \quad \frac{\partial}{\partial y}\left(\frac{\bar{P}_{eff}}{\rho} + \overline{v'^2}\right) = 2\Omega_z \bar{u} \\ z - eq^n \quad &: \quad -\frac{\partial \overline{w'v'}}{\partial y} = 0 \end{aligned} \tag{2.3}$$

Since all velocities and their fluctuations must be zeros at the walls (stick BC); solving continuity and z-momentum equations yields:

$$\begin{aligned} \bar{v} &= 0 \\ \overline{w'v'} &= 0 \end{aligned} \tag{2.4}$$

Furthermore, differentiating y-equation *with respect to* x and x-equation *with respect to* y yields the streamwise pressure gradient , $\frac{\partial}{\partial x}P_{eff}$, to be a constant. Integrating the x-momentum equation from $y = 0$ to $y = 2h$ gives the value of the pressure gradient in terms of wall shear stress (τ_w) as,

$$\begin{aligned} &\frac{\partial}{\partial x}P_{eff} = -\frac{\rho\nu}{h}\left.\frac{\partial \bar{u}}{\partial y}\right|_{y=0} = -\frac{\tau_w}{h} \\ &where, \\ &\tau_w = \rho\nu \left.\frac{\partial \bar{u}}{\partial y}\right|_{y=0} \end{aligned} \tag{2.5}$$

2.2.3 Discussion on scalar eddy viscosity models

Reynolds averaging gives rise to the term $\overline{u_i'u_j'}$ in 2.2. It acts as a *stress* due to velocity fluctuations on the system and hence, is called *Reynold stress* term. In eddy viscosity turbulence models, the net effect of Reynolds stresses is assumed to increase the "*effective*" viscosity of the fluid [6]. This assumption is called the *Boussinesq* assumption, and is represented mathematically as:

$$\overline{u_i'u_j'} = -\nu_t\left(\frac{\partial \bar{u}_i}{\partial x_j} + \frac{\partial \bar{u}_j}{\partial x_i}\right)$$

In the present study Wilcox's two equation k-ω turbulence model has been used for closure [38]. It consists of two partial differential equations (2.6 & 2.7) in two variables, the Turbulent Kinetic Energy (TKE), k, due to velocity fluctuations and the specific rate of dissipation , ω, of TKE into internal thermal energy.

$$\frac{\partial(\rho k)}{\partial t} + \frac{\partial(\rho \bar{u}_j\, k)}{\partial x_j} = P - \alpha^*\rho\omega k + \frac{\partial}{\partial x_j}\left(\left(\mu + \sigma^*\frac{\rho k}{\omega}\right)\frac{\partial k}{\partial x_j}\right) \tag{2.6}$$

$$\frac{\partial(\rho\omega)}{\partial t} + \frac{\partial(\rho\bar{u}_j\,\omega)}{\partial x_j} = \frac{\gamma\omega}{k}P - \alpha\rho\omega^2 + \frac{\partial}{\partial x_j}\left(\left(\mu + \sigma\frac{\rho k}{\omega}\right)\frac{\partial w}{\partial x_j}\right) \tag{2.7}$$

where,

$$\begin{aligned} P &= \tau_{ij}\frac{\partial\bar{u}_i}{\partial x_j} \\ \tau_{ij} &= \mu_t\left(2S_{ij} - \frac{2}{3}\frac{\partial\bar{u}_k}{\partial x_k}\delta_{ij}\right) - \frac{2}{3}\rho k\delta_{ij} \\ S_{ij} &= \frac{1}{2}\left(\frac{\partial\bar{u}_i}{\partial x_j} + \frac{\partial\bar{u}_j}{\partial x_i}\right) \end{aligned} \tag{2.8}$$

The values of constants used in 2.6 and 2.7 have been provided in table 2.1. Once k & ω are evaluated, the eddy viscosity can be computed using:

$$\nu_t = \frac{k}{\omega} \tag{2.9}$$

Table 2.1: Constants in Wilcox's k-ω Model

$\alpha*$	α	γ	$\sigma*$	σ
0.09	$\frac{3}{40}$	$\frac{5}{9}$	0.5	0.5

2.2.4 Effects of rotation on turbulence

Rotation greatly affects the production of turbulent kinetic energy. Fluid elements experience two different kinds of rotations: first, due to system rotation and second, due to mean shear. If the fluid element, due to mean shear, co-rotates with the system (case 1 in figure 2.2), turbulence gets suppressed whereas counter-rotation (case 2 in figure 2.2) enhances it [10]. Due to this difference in the production of TKE, the mean velocity profile becomes asymmetric unlike plane non-rotating channel flow.

2.2.5 Final flow equations and boundary conditions

The x-momentum equation (2.3) together with transport equations for k & ω, after applying steady & homogeneous (in x& z) assumptions, represent the final set of flow equations (2.10a-

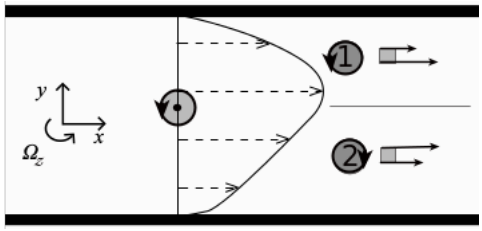

Figure 2.2: Asymmetry due to system rotation
(Original fig. from [17])

2.10c). Mean velocity and TKE must vanish on the walls and, hence, have been subjected to Dirichlet boundary conditions as in outlined in equation 2.11. Specific dissipation has been subjected to asymptotic (as d $\rightarrow$ 0) boundary condition for smooth walls, with $\beta_0 = 0.00708$ and d=distance to nearest wall, as outlined by Wilcox et al. [38].

$$N_1 \equiv -\frac{1}{\rho}\frac{\partial \overline{P}_{eff}}{\partial x} + \frac{\partial}{\partial y}\left((\nu + \nu_t)\frac{\partial \overline{u}}{\partial y}\right) = 0 \tag{2.10a}$$

$$N_2 \equiv \nu_t \left(\frac{\partial \overline{u}}{\partial y}\right)^2 \beta(y) - \alpha^* k\omega + \frac{\partial}{\partial y}\left((\nu + \sigma^* \nu_t)\frac{\partial k}{\partial y}\right) = 0 \tag{2.10b}$$

$$N_3 \equiv \gamma \left(\frac{\partial \overline{u}}{\partial y}\right)^2 - \alpha\omega^2 + \frac{\partial}{\partial y}\left((\nu + \sigma\nu_t)\frac{\partial \omega}{\partial y}\right) = 0 \tag{2.10c}$$

$$\bar{u}|_{y=0} = \bar{u}|_{y=2h} = 0 \tag{2.11a}$$

$$k|_{y=0} = k|_{y=2h} = 0 \tag{2.11b}$$

$$\omega|_{wall} \rightarrow \frac{6\nu_{wall}}{\beta_0 d^2} \tag{2.11c}$$

To solve the flow, pressure gradient is specified in terms of frictional velocity (u_τ) which has been explained in detail in section 3.1. Also, it should be noted that $\beta(y)$ in the production term of k-equation is not a part of the original k-ω model. It has been introduced as an extra parameter and its significance has been explained in the next section.

2.3 Inverse Turbulence Modeling Setup

2.3.1 Introduction

Introduction of the spatial field $\beta(y)$, called *design variable*, in 2.10b sets up turbulent channel flow problem as an *inverse problem*. Different values of β at different grid locations fine tunes the production of TKE which, in turn, changes the eddy-viscosity (ν_t) yielding a different profile for $\bar{u}$. It should, however, be noted that the production term of TKE equation (P_k), unlike other terms in k-ω model, doesn't have a model constant &, hence, treated as an exact term. Moreover, correcting the P_k term without a corresponding correction in eddy-viscosity in the momentum equation violates energy conservation; energy extracted from mean shear by the fluctuations is not in balance with production of TKE [2]. Nevertheless, initial set of simulations for all test cases has been performed by modifying the production term of TKE equation first and extending the *modification* to other terms in 2.10b-2.10c later on. The aim of this section is to elucidate a methodology to obtain a specific distribution of $\beta(y)$ which will increase the accuracy of the RANS model by improving its predicting capabilities.

2.3.2 Turbulence modeling as an optimization problem

The objective of the inverse design is to improve a "model" by predicting certain missing information. This missing information is obtained by making the model to match high fidelity data (either experimental or numerical) for the same flow configurations. An *objective* or *cost* function is defined in terms of *prior* (results from DNS/experiments) and *posterior* variables (model predictions) to give a quantitative measure of the accuracy of turbulence model. Equation 2.12 defines such a function in terms of mean velocity ($\bar{u}$) obtained from the model and velocity obtained from DNS simulation of channel flow (u_{DNS}).

$$F(\vec{u}, \vec{\beta}) = \sum_{i=1}^{n} (\bar{u}_i - u_{DNS_i})^2 \tag{2.12}$$

The definition of F in 2.12 is not limited only to mean velocity. However, attention must be paid to the underlying nature of the turbulence model used. For example, the k-ω model by design under-predicts the TKE production near wall. So, defining an objective function to

match the k profiles of RANS and DNS results in wrong mean velocity profile.

In addition to minimizing 2.12, the flow and design variables must also satisfy the governing flow equations [2.10a-2.10c]. Hence, a formal optimization statement can be defined as:

$$\begin{aligned} &\underset{\beta}{\text{minimize}} \quad F(\vec{u},\vec{\beta}) = \sum_{i=1}^{n} (\bar{u}_i - u_{DNS_i})^2 \\ &\text{Subject to} \quad N(\vec{u},\vec{\beta}) = 0 \\ &\text{where,} \\ &N = [N_1, N_2, N_3]^T \end{aligned} \tag{2.13}$$

Problem 2.13 is a constrained optimization problem which has been solved using deterministic optimization methods. Deterministic optimization methods use gradient of the objective function, $\left(\vec{G} = \frac{\delta F}{\delta \vec{\beta}}\right)$, to update the design variables iteratively,

$$\vec{\beta}^{n+1} = \vec{\beta}^{n} - \alpha * \vec{G} \tag{2.14}$$

where n is the iteration number and α is the step size [4].

2.3.3 The *problem* of gradient calculation

2.3.3.1 *Direct* gradient calculation

The gradient of an objective function, F, with respect to design variable β, is given by

$$\frac{dF}{d\beta} = F_\beta + F_{\vec{u}}\vec{u}_\beta \tag{2.15}$$

F_β & $F_{\vec{u}}$ are easier to calculate as they represent a direct contribution from a variation in design variable and flow variable respectively. However, it is the term $\vec{u}_\beta$ on right hand side that is problematic. To obtain this term the flow equation must be solved. Suppose the flow equations is given by

$$A\vec{u} = f \tag{2.16}$$

Then,

$$\vec{u}_\beta = A^{-1}\left(f_\beta - A_\beta \vec{u}\right) \tag{2.17}$$

Substituting equation 2.17 in 2.15 yields,

$$\frac{dF}{d\beta} = F_\beta + F_{\vec{u}}\left[A^{-1}\left(f_\beta - A_\beta \vec{u}\right)\right] \tag{2.18}$$

The gradient can be obtained by solving equation 2.17 and then substituting it in equation 2.18. If $\beta = \beta_{p\times 1}$, the flow has to be solved p times to obtain the gradient. This strategy is fine as long as p is not very high. But, when β becomes high dimensional, calculating gradient directly becomes numerically prohibitive.

Another strategy is to write 2.18 as

$$\frac{dF}{d\beta} = F_\beta + \left[F_{\vec{u}} A^{-1}\right]\left(f_\beta - A_\beta \vec{u}\right) \tag{2.19}$$

such that substituting

$$\lambda^T = F_{\vec{u}} A^{-1} \tag{2.20}$$

in 2.19 yields:

$$\frac{dF}{d\beta} = F_\beta + \lambda^T\left(f_\beta - A_\beta \vec{u}\right) \tag{2.21}$$

Equation 2.20 can be rearranged as

$$A^T \lambda = F_{\vec{u}}^T \tag{2.22}$$

which is called the *adjoint equation*. Solving 2.22 has similar computational cost as solving another flow equation. So, if m=number of flow variables, the adjoint approach is computationally cheaper than direct gradient calculation when m$\ll$p [22].

2.3.3.2 The *cost* effectiveness of Adjoint Method

The Adjoint method can be understood either through the concept of *duality* or in terms of *Lagrange multipliers* [16]. In this study, the working of adjoints has been explained using Lagrange multipliers.

First, an *augmented* objective function, $I(\vec{u}, \vec{\beta})$, is defined by adding a scalar multiple of flow equations to the original objective function, F [2.23]. Since N=0, a minima in I corresponds to a minima in F. The scalar $\lambda^T \equiv [\lambda_1, \lambda_2, \lambda_3]^T$ is called the *Lagrange multiplier*.

$$I(\vec{u}, \vec{\beta}) \;=\; F(\vec{u}, \vec{\beta}) - \lambda^T N(\vec{u}, \vec{\beta}) \tag{2.23}$$

Taking a variation of 2.23,

$$\delta I(\vec{u}, \vec{\beta}) \;=\; \delta F(\vec{u}, \vec{\beta}) \;-\; \lambda^T \delta N(\vec{u}, \vec{\beta}) \tag{2.24}$$

and noting that variation in I is composed of variations in $\vec{u}$ and $\vec{\beta}$, equation 2.24 can be re-written as:

$$\delta I \;=\; \frac{\partial F}{\partial \vec{u}}\delta\vec{u} + \frac{\partial F}{\partial \vec{\beta}}\delta\vec{\beta} \;-\; \lambda^T \left(\frac{\partial N}{\partial \vec{u}}\delta\vec{u} + \frac{\partial N}{\partial \vec{\beta}}\delta\vec{\beta} \right) \tag{2.25}$$

Separating out the contributions from $\delta\vec{u}$ and $\delta\vec{\beta}$, and dividing throughout by $\delta\vec{\beta}$ yields:

$$\frac{\delta I}{\delta \vec{\beta}} \;=\; \left(\frac{\partial F}{\partial \vec{\beta}} - \lambda^T \frac{\partial N}{\partial \vec{\beta}} \right) + \left(\frac{\partial F}{\partial \vec{u}} - \lambda^T \frac{\partial N}{\partial \vec{u}} \right) \frac{\delta \vec{u}}{\delta \vec{\beta}} \tag{2.26}$$

Equation 2.26 is perfect for noticing the effect of including Lagrange multipliers, λ^T, in this definition of 2.23. A specific choice of λ^T such that

$$\left(\frac{\partial F}{\partial \vec{u}} - \lambda^T \frac{\partial N}{\partial \vec{u}} \right) \;=\; 0 \tag{2.27}$$

circumvents the problem of calculating $\frac{\delta \vec{u}}{\delta \vec{\beta}}$ directly. Equation 2.27 is same as equation 2.22 for $A = \frac{\partial N}{\partial \vec{u}}$. λ, obtained from 2.27, can be used to calculate gradient, $\vec{G}$, by solving:

$$\frac{\delta I}{\delta \vec{\beta}} \;=\; \left(\frac{\partial F}{\partial \vec{\beta}} - \lambda^T \frac{\partial N}{\partial \vec{\beta}} \right) \tag{2.28}$$

2.4 Continuous Adjoint Method Implementation

2.4.1 Introduction

There are two distinct ways of deriving adjoint equations, first by *discrete adjoint implementation* where adjoint equations are obtained directly from discretized flow equation and, second, by *continuous adjoint implementation* where a continuous set of adjoint equations are obtained first and discretized later. In this study, the continuous method has been implemented to arrive at the final adjoint equations.

2.4.2 Derivation of continuous adjoint equations

While equation 2.27 lends itself well for discrete adjoint implementation, a different route has been taken to derive the continuous equations. Integrating equations 2.24 from $y = 0$ to $y = 2h$ yields:

$$\int_0^{2h} \delta I \;=\; \int_0^{2h} \delta F - \int_0^{2h} \lambda_1 \delta N_1 - \int_0^{2h} \lambda_2 \delta N_2 - \int_0^{2h} \lambda_3 \delta N_3 \tag{2.29}$$

The variations in equation 2.29 are composed of variations in *flow* $(\bar{u}, k, \omega)$ and *design* (β) variables. That is,

$$\delta F \equiv (\bar{u}_i - u_{D_i})\, \delta \bar{u}_i \tag{2.30}$$

$$\delta N_1 \equiv \frac{\partial}{\partial y}\left[(\nu + \nu_t)\frac{\partial \delta\bar{u}}{\partial y} + \frac{1}{\omega}\frac{\partial \bar{u}}{\partial y}\delta k - \frac{\nu_t}{\omega}\frac{\partial \bar{u}}{\partial y}\delta\omega\right] \tag{2.31}$$

$$\begin{aligned}\delta N_2 \equiv &\left[\frac{\beta}{\omega}\left(\frac{\partial \bar{u}}{\partial y}\right)^2 - \alpha^*\omega\right]\delta k - \left[\frac{\beta\nu_t}{\omega}\left(\frac{\partial \bar{u}}{\partial y}\right)^2 - \alpha^* k\right]\delta\omega + \nu_t\left(\frac{\partial \bar{u}}{\partial y}\right)^2\delta\beta \\ &+ \frac{\partial}{\partial y}\left[(\nu + \sigma^*\nu_t)\frac{\partial \delta k}{\partial y} + \frac{\sigma^*}{\omega}\frac{\partial k}{\partial y}\delta k - \frac{\sigma^*\nu_t}{\omega}\frac{\partial k}{\partial y}\delta\omega\right] + 2\nu_t\beta\frac{\partial u}{\partial y}\frac{\partial \delta\bar{u}}{\partial y}\end{aligned} \tag{2.32}$$

$$\delta N_3 \equiv 2\gamma\frac{\partial \bar{u}}{\partial y}\frac{\partial \delta\bar{u}}{\partial y} - 2\alpha\omega\delta\omega + \frac{\partial}{\partial y}\left[(\nu + \sigma\nu_t)\frac{\partial \delta\omega}{\partial y} + \frac{\sigma}{\omega}\frac{\partial \omega}{\partial y}\delta k - \frac{\sigma\nu_t}{\omega}\frac{\partial \omega}{\partial y}\delta\omega\right] \tag{2.33}$$

Substituting 2.30-2.33 in 2.29 and integrating (by parts) yields:

$$\int \lambda_1 \delta N_1 \equiv \underbrace{\lambda_1 \left[(\nu + \nu_t) \frac{\partial \delta \bar{u}}{\partial y} + \frac{1}{\omega} \frac{\partial \bar{u}}{\partial y} \delta k - \frac{\nu_t}{\omega} \frac{\partial \bar{u}}{\partial y} \delta \omega \right] \Big|_0^{2h}}_{\text{I}} \underbrace{- (\nu + \nu_t) \frac{\partial \lambda_1}{\partial y} \delta \bar{u} \Big|_0^{2h}}_{\text{II}} + \int \underbrace{\left\{ \frac{\partial}{\partial y} \left[(\nu + \nu_t) \frac{\partial \lambda_1}{\partial y} \right] \delta \bar{u} - \left[\frac{1}{\omega} \frac{\partial \bar{u}}{\partial y} \frac{\partial \lambda_1}{\partial y} \right] \delta k + \left[\frac{\nu_t}{\omega} \frac{\partial \bar{u}}{\partial y} \frac{\partial \lambda_1}{\partial y} \right] \delta \omega \right\}}_{\text{III}} \tag{2.34}$$

$$\int \lambda_2 \delta N_2 \equiv \underbrace{\lambda_2 \left[(\nu + \sigma^* \nu_t) \frac{\partial \delta k}{\partial y} + \frac{\sigma^*}{\omega} \frac{\partial k}{\partial y} \delta k - \frac{\sigma^* \nu_t}{\omega} \frac{\partial k}{\partial y} \delta \omega \right] \Big|_0^{2h}}_{\text{I}} \underbrace{- (\nu + \sigma^* \nu_t) \frac{\partial \lambda_2}{\partial y} \delta k \Big|_0^{2h} + 2\nu_t \beta \lambda_2 \frac{\partial u}{\partial y} \delta \bar{u} \Big|_0^{2h}}_{\text{II}} + \int \underbrace{\nu_t \lambda_2 \left(\frac{\partial \bar{u}}{\partial y} \right)^2 \delta \beta}_{\text{IV}} + \int \underbrace{\left\{ \left[\lambda_2 \left(\frac{\beta}{\omega} \left(\frac{\partial \bar{u}}{\partial y} \right)^2 - \alpha^* \omega \right) + \left(\frac{\partial}{\partial y} \left[(\nu + \sigma^* \nu_t) \frac{\partial \lambda_2}{\partial y} \right] \right) \right] \delta k - \frac{\partial}{\partial y} \left[2\nu_t \beta \lambda_2 \frac{\partial u}{\partial y} \right] \delta \bar{u} - \lambda_2 \left[\frac{\beta \nu_t}{\omega} \left(\frac{\partial \bar{u}}{\partial y} \right)^2 - \alpha^* k \right] \delta \omega \right\}}_{\text{III}} \tag{2.35}$$

$$\int \lambda_3 \delta N_3 \equiv \underbrace{\lambda_3 \left[(\nu + \sigma \nu_t) \frac{\partial \delta \omega}{\partial y} + \frac{\sigma}{\omega} \frac{\partial \omega}{\partial y} \delta k - \frac{\sigma \nu_t}{\omega} \frac{\partial \omega}{\partial y} \delta \omega \right] \Big|_0^{2h}}_{\text{I}} \underbrace{- (\nu + \sigma \nu_t) \frac{\partial \lambda_3}{\partial y} \delta \omega \Big|_0^{2h} + 2\gamma \lambda_3 \frac{\partial \bar{u}}{\partial y} \delta \bar{u} \Big|_0^{2h}}_{II} + \int \underbrace{\left\{ \left[\frac{\partial}{\partial y} \left((\nu + \sigma \nu_t) \frac{\partial \lambda_3}{\partial y} \right) + \frac{\sigma \nu_t}{\omega} \frac{\partial \omega}{\partial y} \frac{\partial \lambda_3}{\partial y} - 2\alpha \lambda_3 \omega \right] \delta \omega - \frac{\partial}{\partial y} \left(2\gamma \lambda_3 \frac{\partial \bar{u}}{\partial y} \right) \delta \bar{u} - \frac{\sigma}{\omega} \frac{\partial \omega}{\partial y} \frac{\partial \lambda_3}{\partial y} \delta k \right\}}_{III} \tag{2.36}$$

Boundary terms II in 2.34-2.36 have no contribution to the integral since the flow variables are subjected to Dirichlet boundary conditions [see equation 2.11]. The adjoint variables must

also vanish on the boundary to nullify the other contribution from boundary integral term (I in 2.34-2.36). Simplifying 2.34-2.36 yields an equation in $\delta\bar{u}$,δk,$\delta\omega$ & $\delta\beta$, which is equivalent to:

$$\int_0^{2h} \delta I = \int_0^{2h} [M_1]\,\delta\bar{u} + \int_0^{2h} [M_2]\,\delta k + \int_0^{2h} [M_3]\,\delta\omega + \int_0^{2h} \left[\vec{G}\right]\delta\beta \tag{2.37}$$

Equating the coefficients $M_1 - M_3$ to zero reduces the variation in I only in terms of β and, consequently, also yields a system of adjoint equations [2.38-2.40] for plane turbulent channel flow with $k-\omega$ closure.

$$M_1 \equiv \frac{\partial}{\partial y}\left[(\nu+\nu_t)\frac{\partial\lambda_1}{\partial y}\right] - \frac{\partial}{\partial y}\left[\left(2\beta\nu_t\frac{\partial\bar{u}}{\partial y}\right)\lambda_2\right] - \frac{\partial}{\partial y}\left[\left(2\gamma\frac{\partial\bar{u}}{\partial y}\right)\lambda_3\right] = -(\bar{u}-u_D) \tag{2.38}$$

$$\begin{aligned} M_2 \equiv \left[-\frac{1}{\omega}\frac{\partial\bar{u}}{\partial y}\frac{\partial\lambda_1}{\partial y}\right] + \frac{\partial}{\partial y}\left[(\nu+\sigma^*\nu_t)\frac{\partial\lambda_2}{\partial y}\right] - \frac{\sigma^*}{\omega}\frac{\partial k}{\partial y}\frac{\partial\lambda_2}{\partial y} + \left(\frac{\beta}{\omega}\left(\frac{\partial\bar{u}}{\partial y}\right)^2 - \alpha^*\omega\right)\lambda_2 \\ - \left[\frac{\sigma}{\omega}\frac{\partial\omega}{\partial y}\frac{\partial\lambda_3}{\partial y}\right] = 0 \end{aligned} \tag{2.39}$$

$$\begin{aligned} M_3 \equiv \left[\frac{\nu_t}{\omega}\frac{\partial\bar{u}}{\partial y}\frac{\partial\lambda_1}{\partial y}\right] + \left[-\left(\beta\frac{\nu_t}{\omega}\left(\frac{\partial\bar{u}}{\partial y}\right)^2 + \alpha^* k\right)\lambda_2 + \sigma^*\frac{\nu_t}{\omega}\frac{\partial k}{\partial y}\frac{\partial\lambda_2}{\partial y}\right] \\ + \left[\frac{\partial}{\partial y}\left[(\nu+\nu_t)\frac{\partial\lambda_3}{\partial y}\right] + \sigma\frac{\nu_t}{\omega}\frac{\partial\omega}{\partial y}\frac{\partial\lambda_3}{\partial y} - 2\alpha\omega\lambda_3\right] = 0 \end{aligned} \tag{2.40}$$

Once again, equations 2.38-2.40 have been solved using homogeneous boundary conditions for λ's. Finally, gradient is obtained (from IV in 2.35) by solving:

$$\vec{G} = \frac{\delta I}{\delta\beta} = \nu_t\lambda_2\left(\frac{\partial\bar{u}}{\partial y}\right)^2 \tag{2.41}$$

In many cases, an assumption of "frozen" eddy viscosity [13] in turbulence model has been made to arrive at a different set of adjoint equations; *frozen* in the sense that ν_t is assumed to be constant in the k-ω model but not in the mean flow equation. One of the points of concern is that this assumption might have a significant influence on calculated sensitivity information [41]. However, making this assumption results in a simplified formulation of continuous adjoint method, resulting in equations (outlined in appendix A) which are easier to implement

numerically. Moreover, the inverse results obtained using this assumption, as demonstrated in chapter 4, have been found to be quite good and their use, at least for channel flow, can be justified.

2.4.3 Inverse design cycle

Finally, figure 2.3 provides a schematic for the inverse design process that has been used in this study. Firstly, starting with an initial guess, β_{prior}, the flow equations have been solved to obtain updated values of flow variables ($\vec{u}_{n+1}$). Then, these flow solutions have been used to solve the adjoint equation [2.27]. Lastly, gradient calculated using $\vec{\lambda}_{n+1}$, via equation 2.28, has been used to update the value of β_n according to equation 2.14 to obtain an updated value, β_{n+1}. The cycle is continued until an optimal solution ($\beta_{posterior}$) is reached.

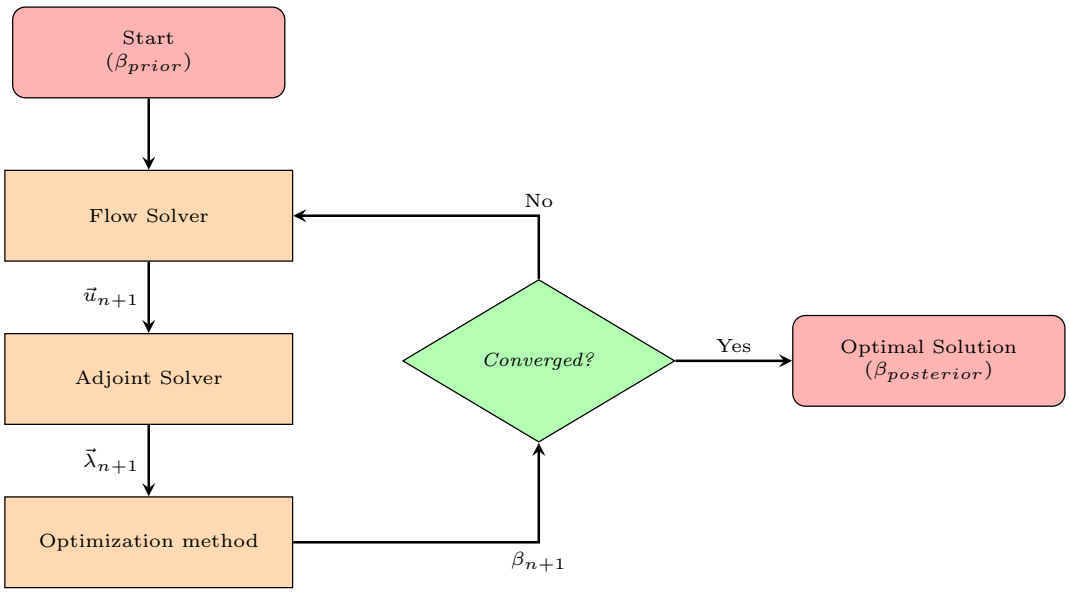

Figure 2.3: Schematics for Inverse Design Process.

2.4.4 Discussion on optimization methods used

After gradient calculation, the next step is to update β according to 2.14. For this thesis, steepest-descent method, where α in 2.14 is a constant, was used. In some *stiff* cases, smoothed variation of the steepest-descent method [20] was also used to achieve a better control over the convergence properties. The smoothed gradient, $\bar{\vec{G}}$, can be obtained from gradient, $\vec{G}$, by solving

$$\bar{\vec{G}} - \frac{\partial}{\partial y}\left(\epsilon \frac{\partial \bar{\vec{G}}}{\partial y}\right) = \vec{G} \tag{2.42}$$

with homogeneous boundary conditions. A small value of ϵ ($\equiv 10^{-3}$) is chosen to maintain accuracy.

2.4.5 Discussion on regularization

Gradient, as given by equation 2.41, depends on velocity gradient. If the velocity gradient is zero, the flow becomes insensitive to β. So, theoretically, any changes in β at those locations will not change the velocity field [8]. This makes the inverse problem *ill-posed*. To make this problem *well-posed* again, it is necessary to provide some additional information.

One way of making the problem well-posed is by Regularization [14]. This is achieved by introducing an additional term, called *penalty factor*, in the objective function definition. One such regularization term is shown in equation 2.43, where objective function is penalized if distribution of β changes from its prior value, β_{prior}, when gradient information is zero.

$$F\left(\vec{u}, \beta\right) = \sum_{i=1}^{N} \left(\bar{u}_i - u_{DNS_i}\right)^2 + C_\beta \sum_{i=1}^{N} \left(\beta_i - \beta_{prior_i}\right)^2 \tag{2.43}$$

The regularization term seems to have no effect on the inversion results for channel flow when used with k-ω turbulence model and it has been included in the definition of F only to make the inverse problem *mathematically* well-posed. The coefficient C_β has been chosen to be small ($\sim 10^{-4}$). However, including a regularization term when eddy viscosity itself is treated as a design variable (for comparison purposes) smooths the inversion result. For that case, a value of $C_\beta = 10^{-3}$ has been found to yield good results.

Since the additional term in 2.43 is defined only in terms of design variable (β), the adjoint equations remain unchanged.

CHAPTER 3. NUMERICAL FRAMEWORK

3.1 Specifying Pressure Gradient

A constant pressure gradient has been applied in the stream-wise direction. Defining frictional velocity, u_τ,

$$u_\tau^2 = \tau_w = \rho\nu \left.\frac{\partial \bar{u}}{\partial y}\right|_{y=0} \tag{3.1}$$

such that the pressure gradient can be expressed in terms of u_τ as,

$$\frac{\partial \bar{p}_{eff}}{\partial x} = -\frac{u_\tau^2}{h} \tag{3.2}$$

where u_τ is used in the definition of friction velocity Reynolds number, $Re_\tau = \frac{u_\tau h}{\nu}$. For a given Re_τ, a fixed value of $u_\tau = 1$ has been used.

3.2 FDM Discretization

The flow and adjoint equations have been solved using an iterative convergence approach with implicit euler scheme. For example, 3.3 represents the evolution equation for λ_1 written in terms of values at n^{th} and $n{+}1^{th}$ iteration steps. Starting with an initial guess, values are calculated using 3.3 until convergence is reached.

$$\begin{aligned}\frac{\partial}{\partial y}\left[(\nu+\nu_t)\frac{\partial \lambda_1}{\partial y}\right]\Bigg|^{n+1} = \frac{\lambda_1^{n+1}-\lambda_1^n}{\Delta t} - (\bar{u}-u_D)|^n + \frac{\partial}{\partial y}\left[\left(2\beta\nu_t\frac{\partial \bar{u}}{\partial y}\right)\lambda_2\right]\Bigg|^n \\ + \frac{\partial}{\partial y}\left[\left(2\gamma\frac{\partial \bar{u}}{\partial y}\right)\lambda_3\right]\Bigg|^n\end{aligned} \tag{3.3}$$

The partial derivatives in 3.3 have been approximated using 2^{nd} order central finite differences shown in equation 3.4, where $\Delta_2 y_j = y_{j+1} - y_{j-1}$ & $\Delta y_j = y_j - y_{j-1}$.

$$\frac{\partial}{\partial y}\left[\alpha\frac{\partial T}{\partial y}\right] \approx \frac{2}{\Delta_2 y_j}\left[\alpha_{j+\frac{1}{2}}\left(\frac{T_{j+1}-T_j}{\Delta y_{j+1}}\right) - \alpha_{j-\frac{1}{2}}\left(\frac{T_j - T_{j-1}}{\Delta y_j}\right)\right] \tag{3.4}$$

The resulting tri-diagonal matrices have been solved using Thomas algorithm[1].

CHAPTER 4. RESULTS

4.1 Introduction

In this chapter, the solver performance results together with the simulation results have been presented. The inverse turbulence modeling methodology, as outlined in chapters 2 & 3, has been implement in two stages. In first stage, the inverse modeling approach has been implemented to *non*-rotating channel flow case for different friction Reynolds numbers. Results have been plotted against different parameters to see if they collapse in a meaningful way. In second stage, the implementation has been extended to rotating channel flow case. Traditionally, DNS of rotating case is based on rotation number (Ro_b), defined using bulk mean velocity ($\bar{U}_b$) as,

$$Ro_b = \frac{2\,|\Omega_z|\,h}{\bar{U}_b} \tag{4.1}$$

Simulations for rotating case have been carried out in two different sets. First set of simulations with spanwise rotation have been performed for rotation number ranging from Ro_b=0.0 to 0.5 with Re_τ=194. This corresponds to the DNS data of Kristoffersen and Andersson [23]. For the second set, higher rotation numbers (Ro_b=0.77 to 3.0) have been considered, with Re_τ=180, using the DNS data of Grundestam et al. [17]. Such high values of Ro_b causes re-laminarization of the flow such that turbulence model becomes less and less sensitive to any changes in design variable.

4.2 Solver Performance

Figures 4.1a-4.1c shows three log-linear plots that demonstrate the performance of the flow solver, adjoint solver and optimization method respectively. "Residual" in fig. 4.1 is the $\|L\|_2$

norm of solutions at two consecutive iterations. As mentioned earlier, figs. 4.1a and 4.1b show that the computational cost of solving an adjoint equation is equivalent to solving one additional flow equation.

The optimal solution is supposed to have been reached when the change in objective function value at two consecutive iterations becomes small ($< 10^{-6}$ in this case). The total cost of inversion, as shown in fig. 4.1c, is equal to solving 8000 iterations of each of primal/flow and adjoint equations. As will be shown later, 2-to-4 orders of magnitude reduction has been achieved in the net objective function value, depending on the problem.

The CPU time for the complete optimization cycle is shown in fig. 4.1d. More number of flow and adjoint iterations are required for convergence at the beginning of the cycle, hence, the time taken is relatively more. The total CPU time taken is around 9.092 seconds. Since the problems considered in this thesis are pseudo one-dimensional, the required CPU time have been found to be very small to warrant any use of code parallelization. It should however be noted that the scenario will be quite different for complicated problems with large number of grid points and code parallelization might become a necessity.

4.3 Inverse Results For Non-rotating Channel Flow

Results for *non*-rotating channel have been obtained using the DNS data of Moser et al. [24]. Three different values of Re_τ, 180, 390 & 590, have been used with 65, 129 & 129 half-channel grid points, respectively.

Figure 4.2 gives the comparison of the inverse solution with DNS data (for $Re_\tau = 590$). For these results, β has been included in the production term of k-equation. The axes are shown in "*plus*" units; wherein $\bar{u}$ and k are scaled using u_τ, and y_+ is defined as:

$$y^+ = \frac{y u_\tau}{\nu} \tag{4.2}$$

The *posterior* result for mean velocity, in 4.2a, matches excellently with DNS data. As the objective function, I, is solely in terms of $\bar{u}$, there is not much improvement in the k profile (figure 4.2b). However, due to the intrinsic nature of a scalar eddy viscosity models, any effort

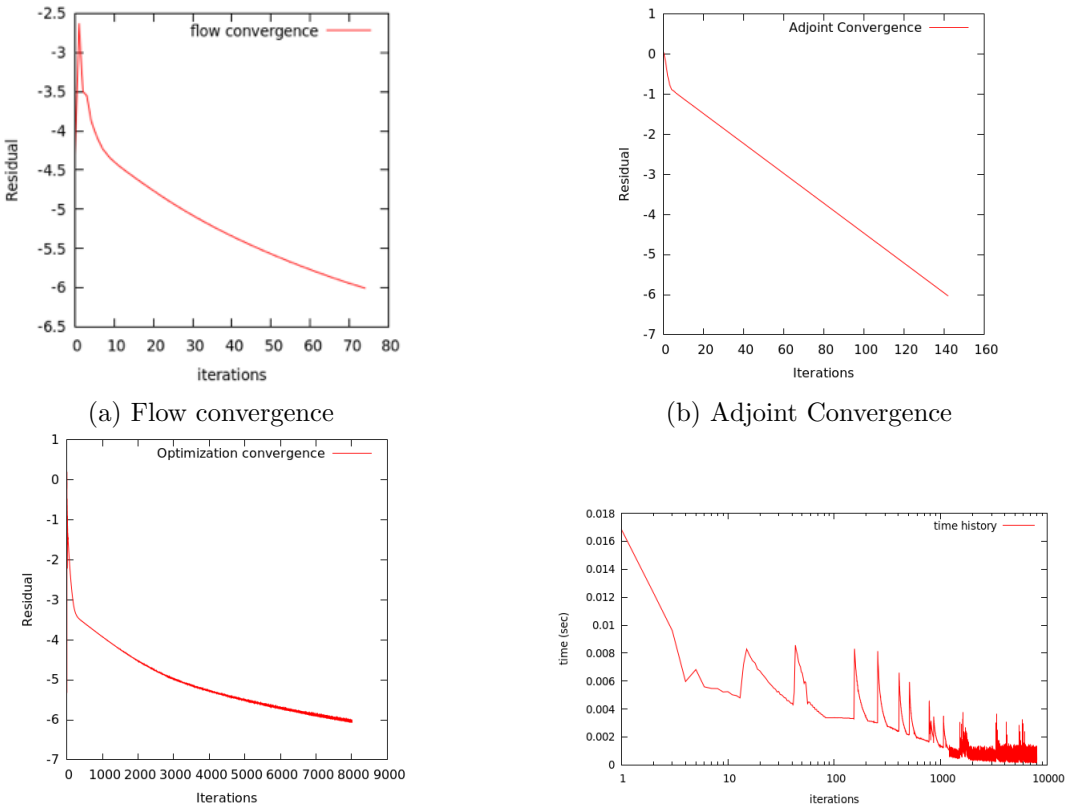

(a) Flow convergence

(b) Adjoint Convergence

(c) Flow convergence

(d) CPU time history

Figure 4.1: Solver Performance

to improve TKE profile, by including it in the definition of I, has been found to yield a wrong mean velocity profile. Results for such an effort (with $I = \sum_{i=1}^{n}(k_i - k_{DNS_i})^2$) have been demonstrated in appendix B, where the inverse result for TKE matches quite well with DNS data but a wrong mean velocity profile is obtained as a consequence. Therefore, to maintain the accuracy of the inverse results for mean velocity, simulations have been performed using only $\bar{u}$ in objective function definition. Reduction of approximately 2 orders in objective function value has been achieved, as shown in figure 4.2d.

The summary of inferred β is shown in figure 4.2c. $\beta = 1.0$ serves as the *prior* or base model for these results. Since the production of k is negligible in viscous sublayer ($y+ < 5$), there is negligible sensitivity to changing β. For verification of the code, β has also been included in the destruction term of TKE equation. Destruction term is physically inverse of production; hence β in destruction comes out as a mirror image of β in production.

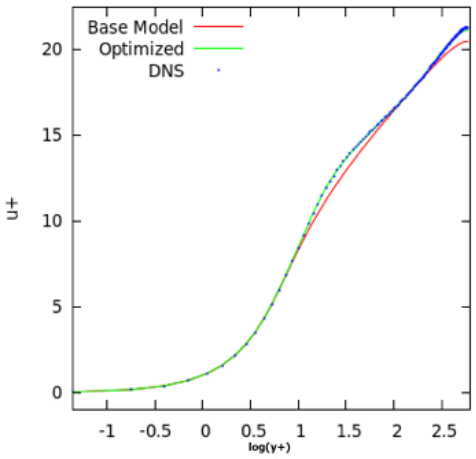

(a) Mean Velocity Profile

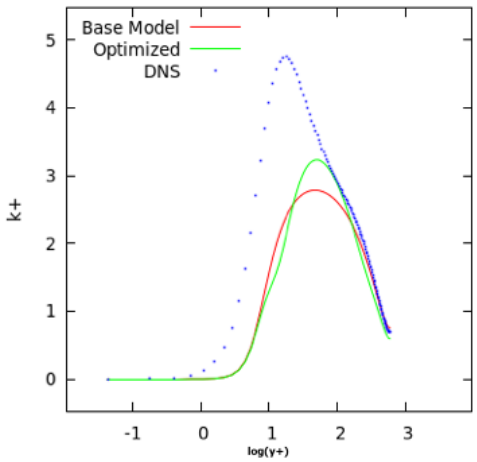

(b) TKE Profile

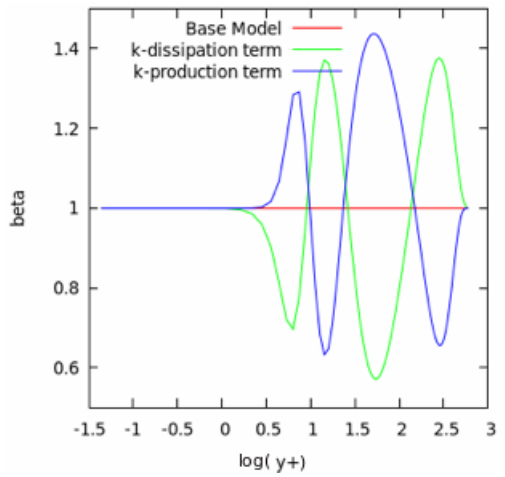

(c) β Profiles

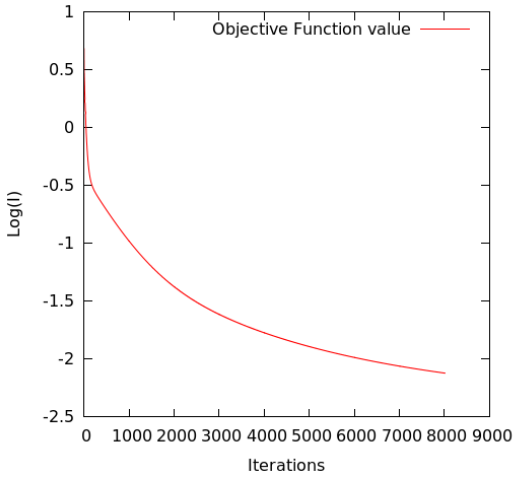

(d) Objective Function Value

Figure 4.2: Inverse solution of non-rotating channel flow with $Re_\tau = 590$

Identifying scaling parameters for these inverse results can be of vital importance for future turbulence model development [27]. In figure 4.3, the inferred β has been plotted against three different parameters as suggested by Parish and Duraisamy [26]: the normalized wall distance (y^+), the wall-normal distance (y) and the turbulent Reynolds number (Re_T) defined as

$$Re_T = \frac{\nu_t}{\nu} \tag{4.3}$$

The scaling of β with $y+$ (fig. 4.3a) and with Re_T (fig. 4.3c) is excellent in the inner region ($y \leq 0.1h$). For $y > 0.6$, fig. 4.3b shows that wall-normal distance, y, becomes the correct scaling parameter.

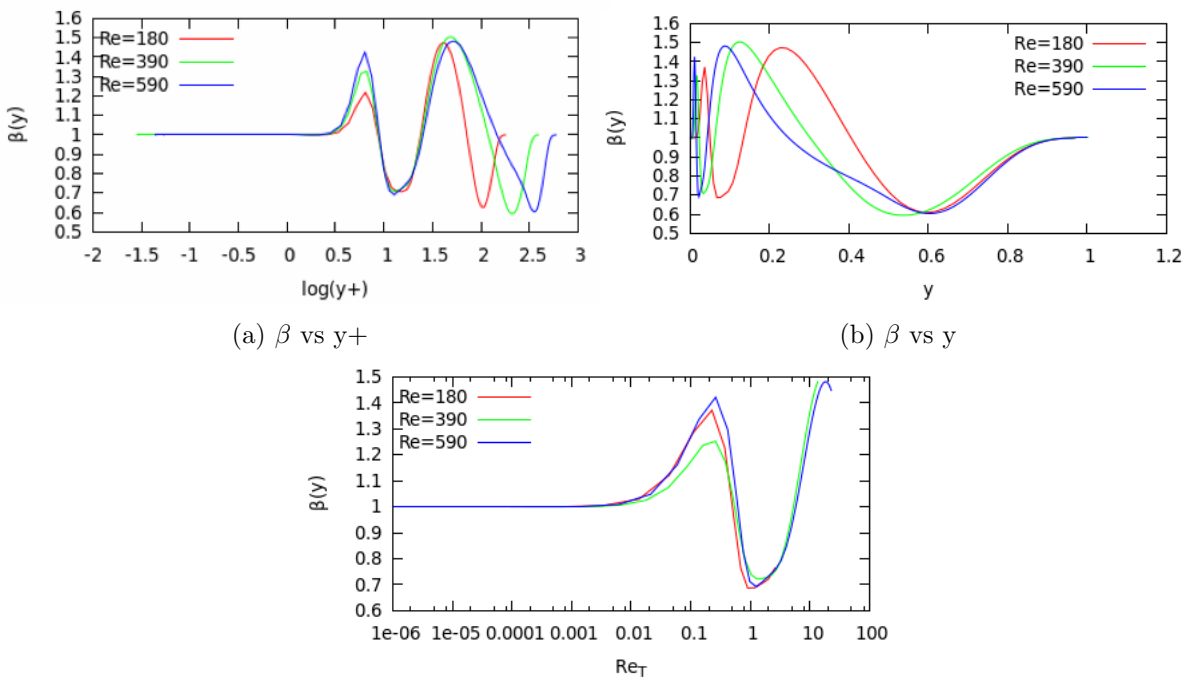

(a) β vs y+

(b) β vs y

(c) β vs Re_T for $y \leq 0.1h$

Figure 4.3: β (in k-production) profiles for different Re_τ

4.4 Channel Flow With Spanwise Rotation

Studying turbulent channel with spanwise rotation has been the primary aim of this study. As discussed, rotation suppresses turbulence in one half and enhances it in the other half of the channel (refer section 2.2.4). Due to this mismatch between TKE production, an asymmetry appears and, hence, calculations have been performed using full channel grid points. Inverse results for rotating channel flow have been presented in the following sections in two different sets, based on Ro_b, to maintain clarity.

4.4.1 Simulation results for low-to-modest rotation numbers

Figure 4.4 shows the inverse velocity profiles, for rotation number ranging from Ro_b=0.0 to 0.5 with Re_τ=194, together with the base model and the actual DNS data from Kristoffersen and Andersson [23]. β has been included in the production term of k-equation for these results. The inverse solution agrees well with DNS data for all cases, except for a very narrow region where curvature in mean velocity changes. This might be, perhaps, due to low sensitivity of β

(because velocity gradients are negligible). 1-3 orders of magnitude reduction has been achieved in objective function value for these cases as shown in fig. C.1 of appendix C. Base model of $\beta = 1.0$ serves quite well to reach the optimum in all the cases.

The distributions of β when included in TKE production and other different terms of k-ω model are shown in figures 4.5 and 4.7, with respect to y and y^+ respectively. One of the major issue with these distributions is the *un-physical* nature of the correction terms, due to the prediction of a *negative* production/destruction terms. This can be avoided by setting a lower limit for β in the model. However, current simulations have been performed without any such limiters as they have been found to reduce the inverse solution accuracy. The un-physical nature of these distributions might become a limiting factor in extracting the *modeling knowledge* based on the scaling parameters thus obtained.

Unlike non-rotating case, scaling parameters for rotating flows are not very clear. β doesn't seem to scale with y at all, however, β in 4.7 does seems to display some similarities with y^+, close to the wall. Though, away from the wall patterns are again not very clear.

The inversion works by altering the eddy viscosity distribution in the domain. In a separate set of simulations, eddy-viscosity itself has been chosen as a *design* variable, to obtain an *optimum* distribution for ν_t without any turbulence model. Figure 4.6 shows the inverse distributions of ν_t with and without a turbulence model for $Ro = 0, 5$ case. These distributions are quite similar on the *unstable* side of the channel but deviate on the *stable* side. This is due to the insensitivity of objective function, with respect to change in design variable, in the region where velocity gradient is zero (refer fig. 4.4f).

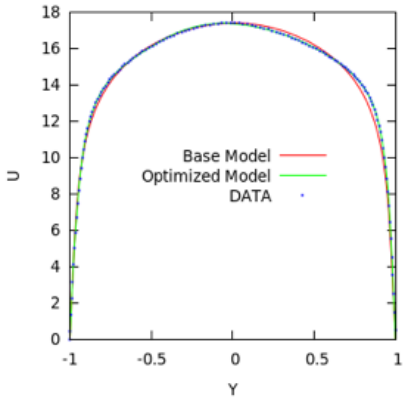

(a) $Ro_b = 0.01$

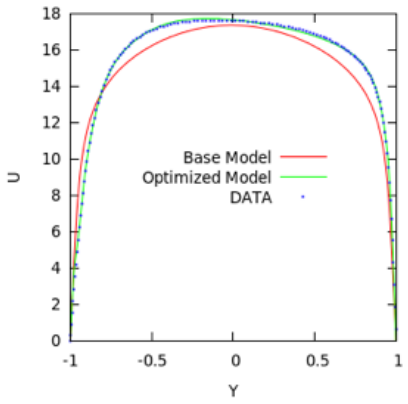

(b) $Ro_b = 0.05$

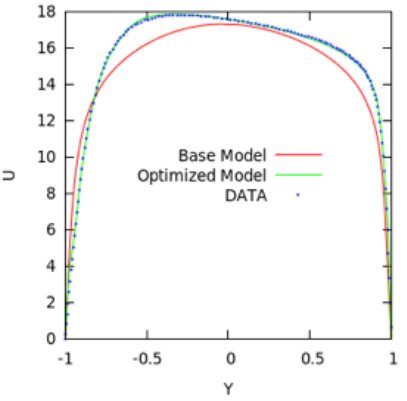

(c) $Ro_b = 0.10$

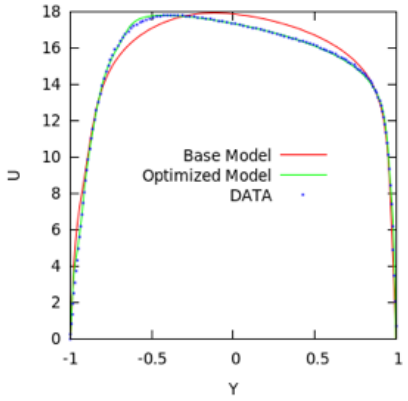

(d) $Ro_b = 0.15$

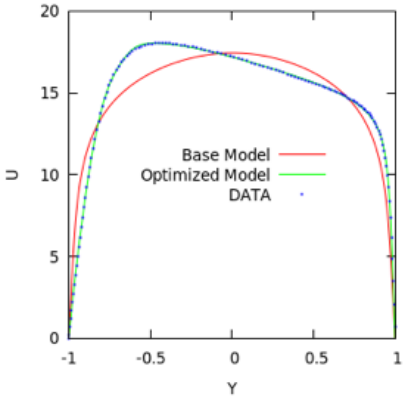

(e) $Ro_b = 0.2$

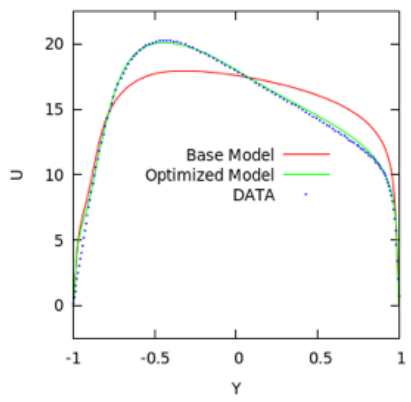

(f) $Ro_b = 0.5$

Figure 4.4: Channel flow with weak-to-moderate spanwise rotation corresponding to DNS data of Kristoffersen *et al.* (1993)

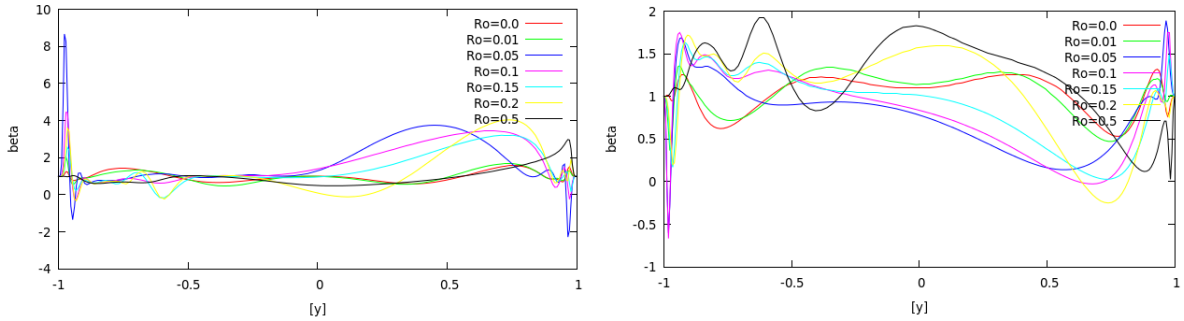

(a) β Profiles for k-production

(b) β Profiles for k-dissipation

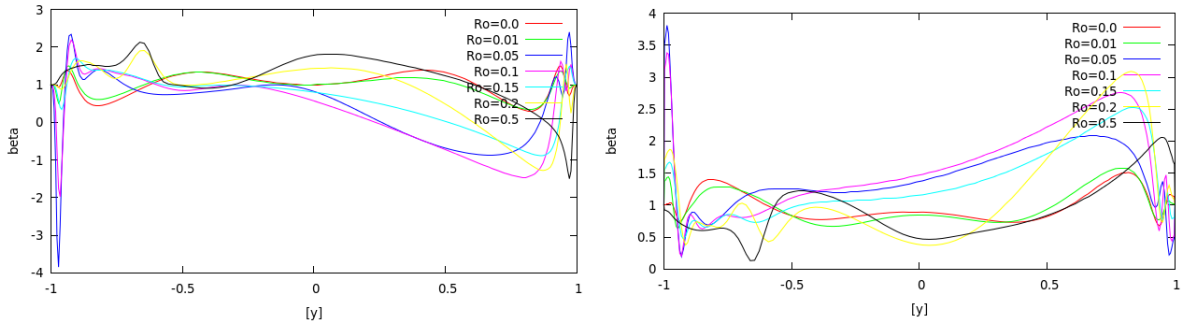

(c) β Profiles for ω-production

(d) β Profiles for ω-dissipation

Figure 4.5: β vs y for different terms

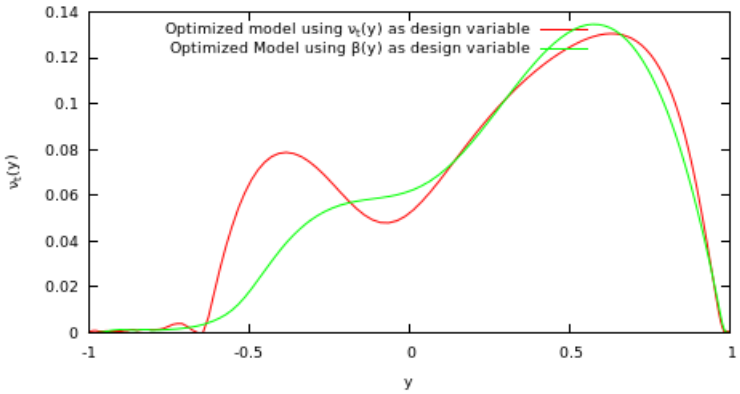

Figure 4.6: Eddy Viscosity (ν_t) distributions for different choice of design variables for $Ro_b = 0.5$ case

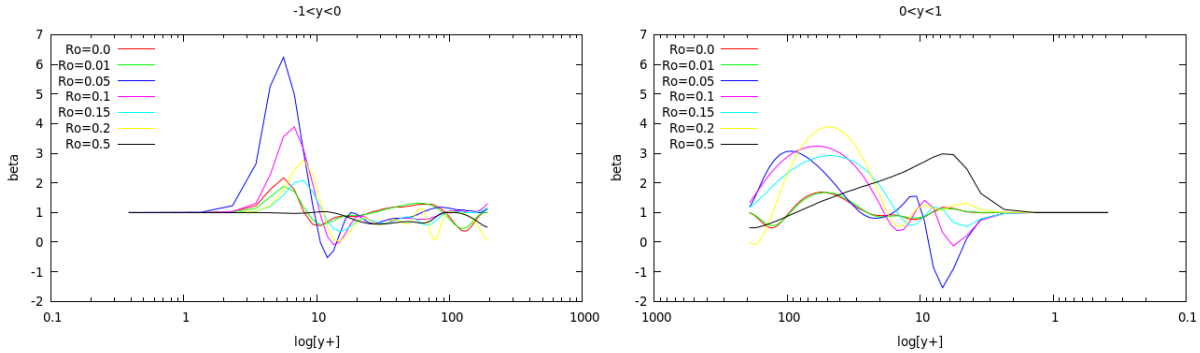

(a) β Profiles for k-production

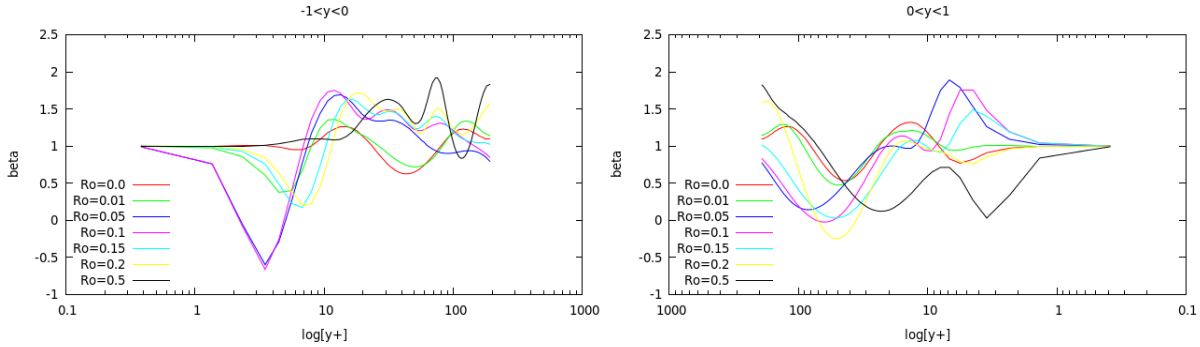

(b) β Profiles for k-dissipation

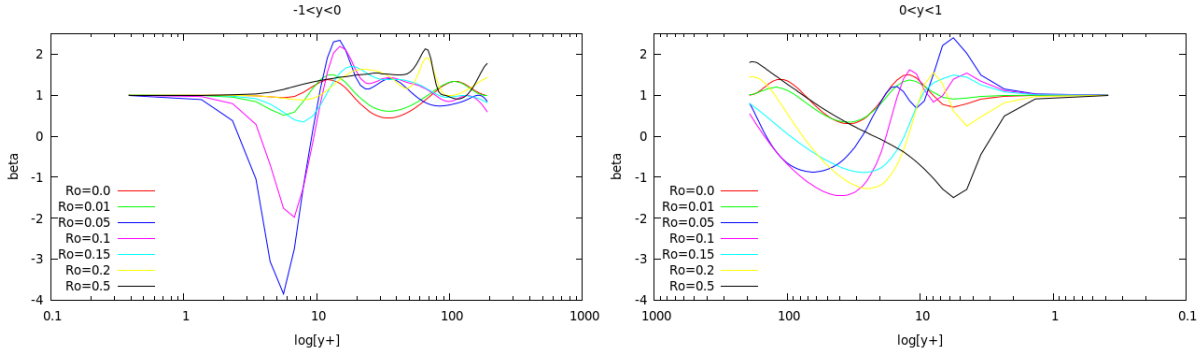

(c) β Profiles for ω-production

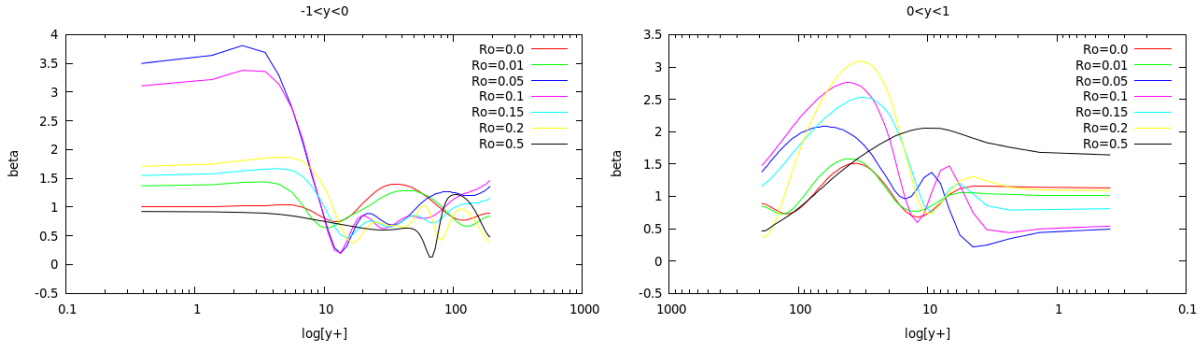

(d) β Profiles for ω-dissipation

Figure 4.7: β vs y+ for different terms

4.4.1.1 Comparison to *Hellsten* F_4 model

Hellsten [18] modified the ω transport equation in SST variation of $k-\omega$ model to sensitize it to rotation and curvature effects. Coefficient F_4 included in the $\omega-$destruction term ($D_\omega = F_4\beta\omega^2$) is given a parametric dependence on rotation by defining it as:

$$F_4 = \frac{1}{1 + C_{rc}Ri}$$
$$\text{where,} \tag{4.4}$$
$$Ri = -2\Omega_z\left(\frac{\partial\bar{u}}{\partial y} - 2\Omega_z\right)\Bigg/\left(\frac{\partial\bar{u}}{\partial y}\right)^2$$

where, $C_{rc} = 3.6$. Figure 4.8 gives a comparison of correction coefficients and mean velocity distributions obtained through Hellsten's and the present model.

The corroboration between the correction coefficients for the two models is poor as seen in fig. 4.8a, except for a narrow region in the unstable region at higher rotation numbers for which the F_4 model might not be valid at all [18]. The stable region where flow achieves a zero gradient of velocity is problematic for both the models due to the insensitivity of coefficients.

4.4.2 Simulation results for modest-to-high rotation numbers

Second set of simulations have been performed for rotation number ranging from Ro_b=0.77 to 3.0 with Re_τ=180. The inverse solution has, again, been found to be in an excellent agreement with the data as shown in figure 4.9. The parabolic nature of DNS mean velocity profiles in 4.9f-4.9f suggests the laminarizing effect of strong spanwise rotations.

Figure 4.10 shows the distribution of β when it has been included in production term of k-equation.The inverse model has been found to be severely affected by the presence of *local minimums* for these rotation numbers. The existence of these local minimums have restricted the use of $\beta = 1$ as the base model for many cases. Thus, wherever necessary, inverse result from previous Ro_b case has been used as the base model for new Ro_b. β is tending towards a symmetric profile as the rotation numbers goes closer to $Ro_b = 3.00$, which follows from the parabolic nature of the inverse solution for higher rotations in 4.9e & 4.9f to match the data.

The *posterior* distributions of turbulent kinetic energy (TKE), specific dissipation rate and eddy-viscosity have been provided in figure 4.11. With increasing rotation number, laminarizing effect of rotation becomes profound according to the phenomenology explained in 2.2.4. This is evident from figures 4.11a & 4.11c, where, TKE & ν_t decrease substantially until, at $Ro_b = 3.0$, they are almost zero across the channel; hence the parabolic profile. Change in specific dissipation (figure 4.11b) with increasing Ro_b is relatively small and it tends towards a more symmetric profile. Also, for rotation rates closer to laminar limit, the sensitivity of $\bar{u}$ with changing β is almost non-existent and model effectively stops working at $Ro_b = 3.0$. This has been verified by inverse modeling the laminar channel flow profile, at $Re_\tau = 180$, for which no further improvement was observed.

The *posterior* distributions of β, when included in various different model transport equation terms, have been plotted in figures 4.12 (w.r.t y) and 4.13 (w.r.t. y^+). Except for rotation numbers of 2.49 & 3.0, β seems to scale with normalized wall distance, y^+ (fig:4.13). But, since the sensitivity has been diminished, inverse results for rotation numbers closer to laminar limit might not be useful for turbulence modeling at all.

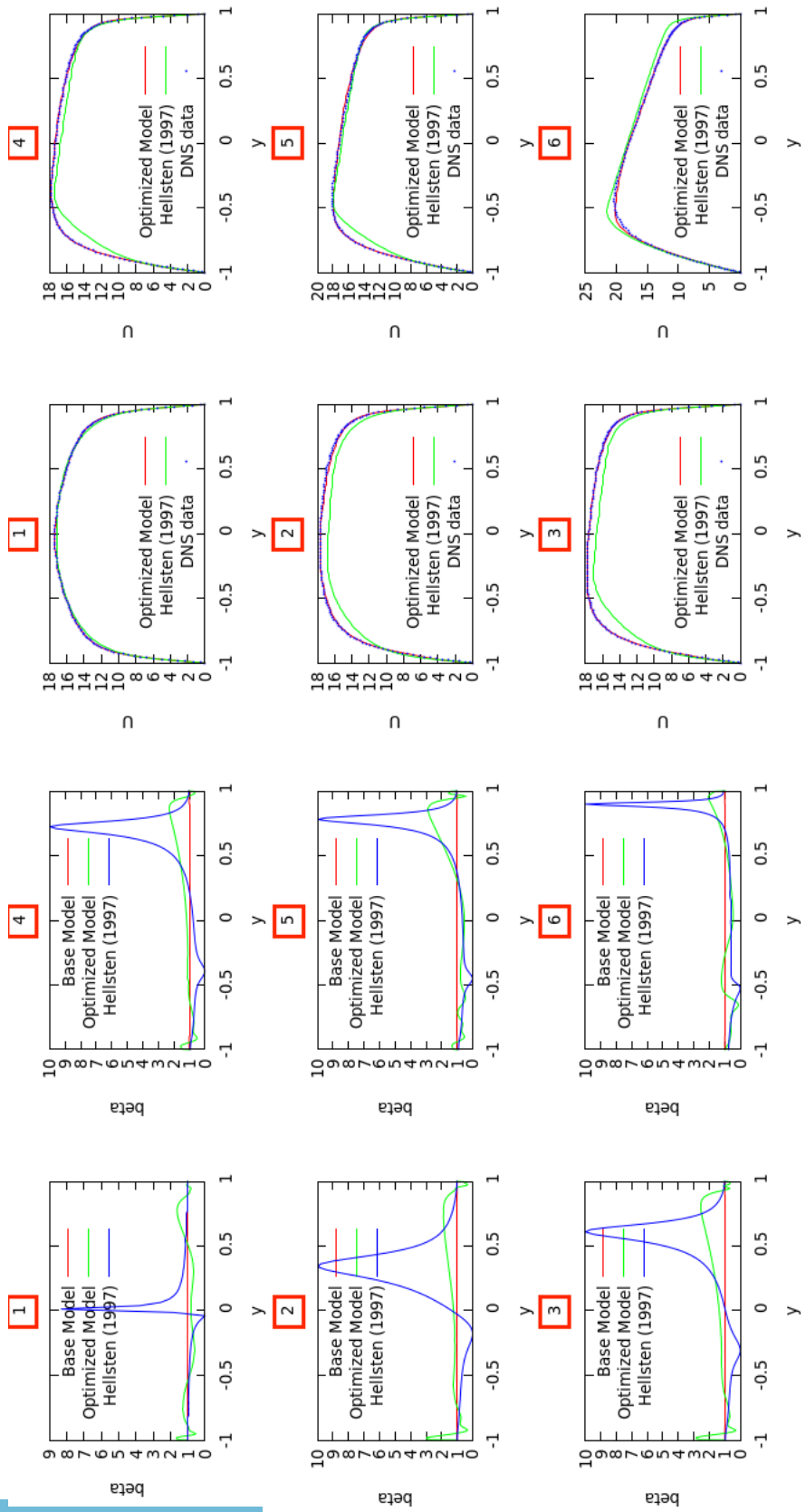

(a) *Correction* coefficient (β & F_4) plots

(b) Mean velocity profiles

Figure 4.8: Validation results for *Hellsten* (1971). Labels 1-6 represent the following rotation rates (in brackets): 1(0.01), 2(0.05), 3(0.1), 4(0.15), 5(0.2) & 6(0.5)

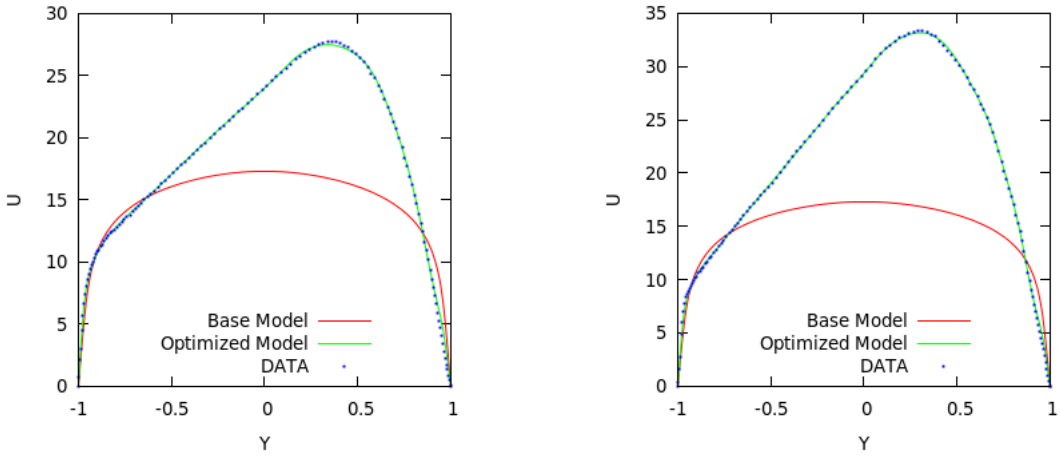

(a) $Ro_b = 0.77$

(b) $Ro_b = 0.98$

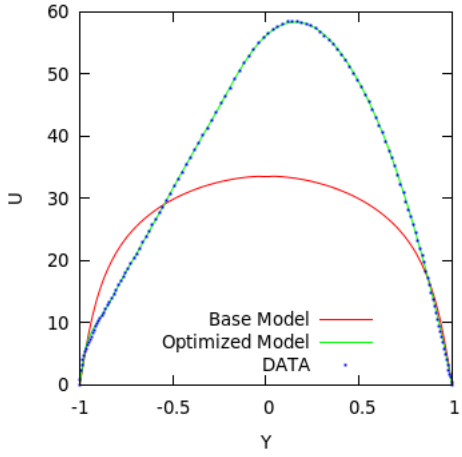

(c) $Ro_b = 1.5$

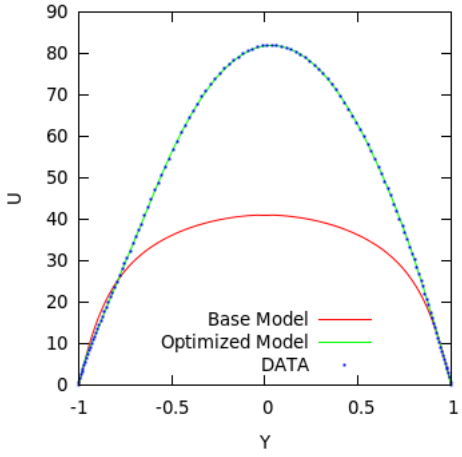

(d) $Ro_b = 2.06$

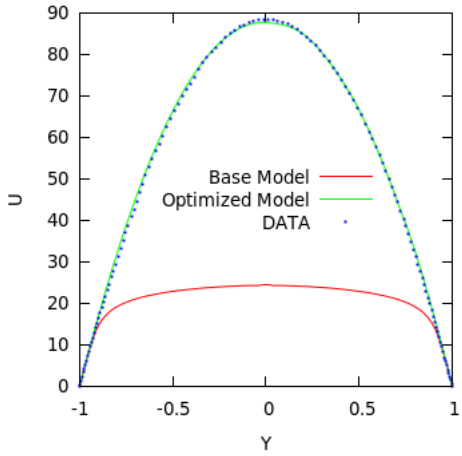

(e) $Ro_b = 2.49$

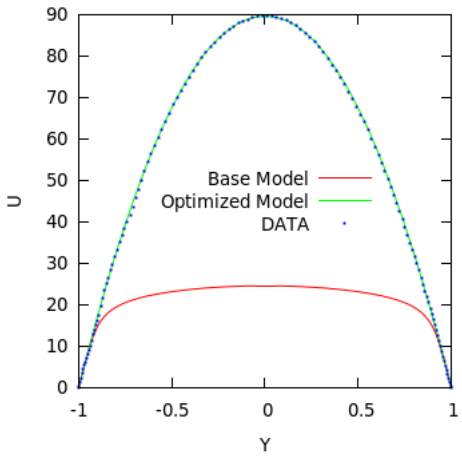

(f) $Ro_b = 3.00$

Figure 4.9: Channel flow with moderate-to-strong spanwise rotation corresponding to DNS data of Grundestam *et al.* (2008)

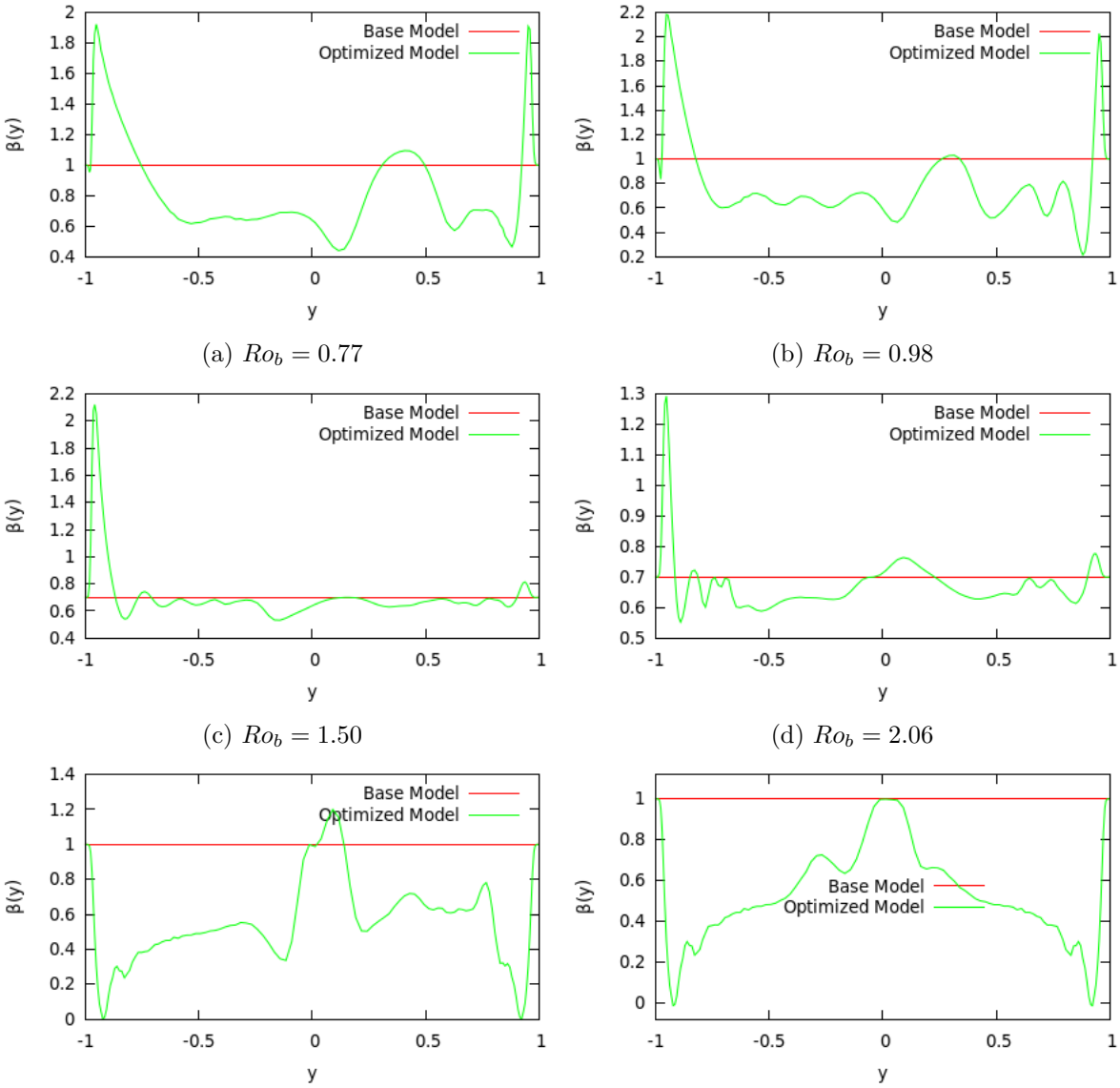

(a) $Ro_b = 0.77$

(b) $Ro_b = 0.98$

(c) $Ro_b = 1.50$

(d) $Ro_b = 2.06$

(e) $Ro_b = 2.49$

(f) $Ro_b = 3.00$

Figure 4.10: β (k-production term) profiles for Grundestam *et al.* (2008)

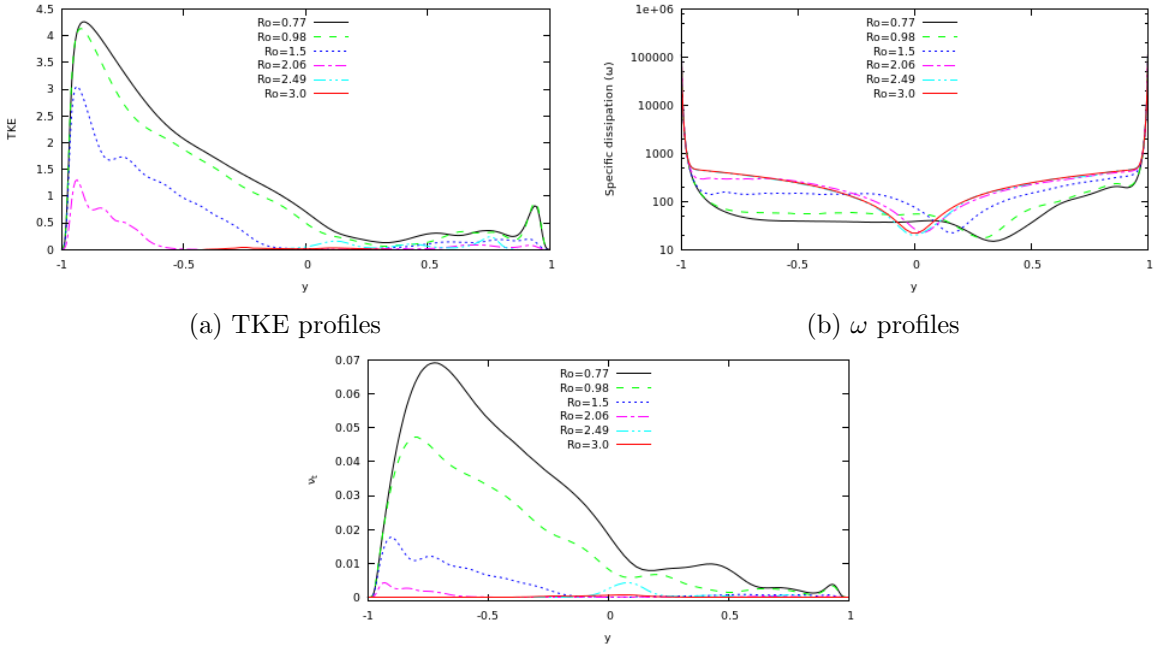

(a) TKE profiles

(b) ω profiles

(c) ν_t profiles

Figure 4.11: TKE, Specific dissipate rate (ω) & eddy-viscosity (ν_t) plots for DNS cases of Grundestam *et al.* (2008) ($0.5 < Ro_b \leqslant 3.0$)

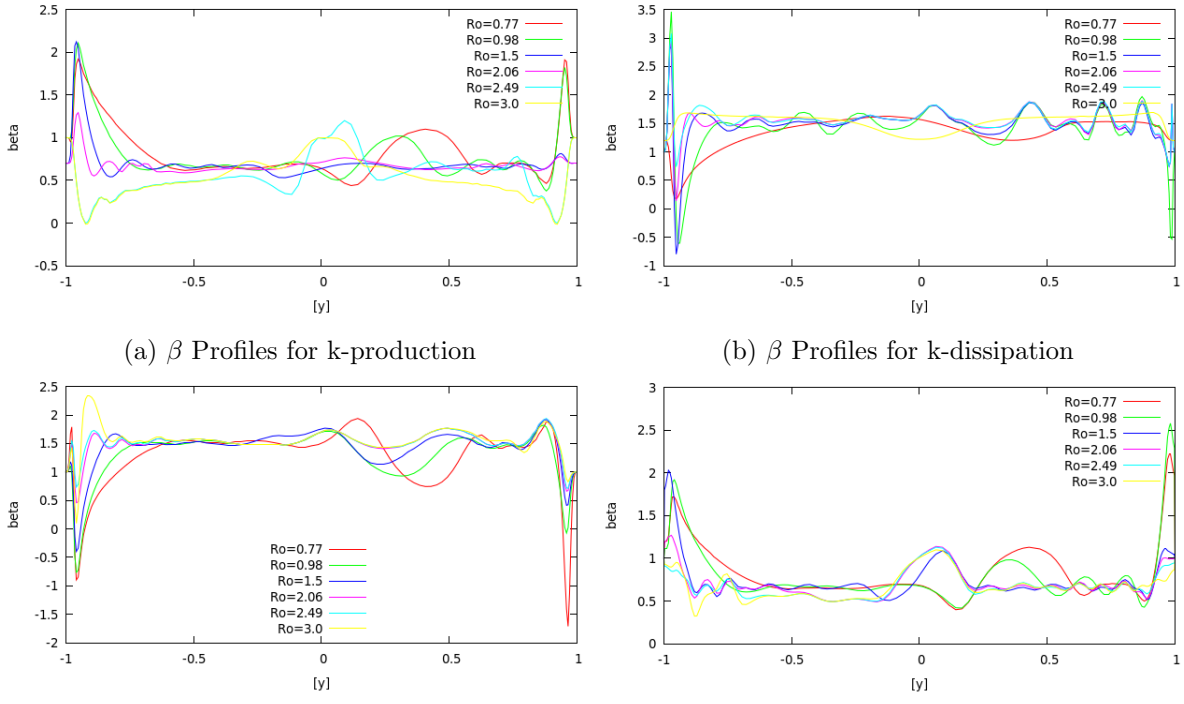

(a) β Profiles for k-production

(b) β Profiles for k-dissipation

(c) β Profiles for ω-production

(d) β Profiles for ω-dissipation

Figure 4.12: β vs y for DNS cases of Grundestam *et al.* (2008)

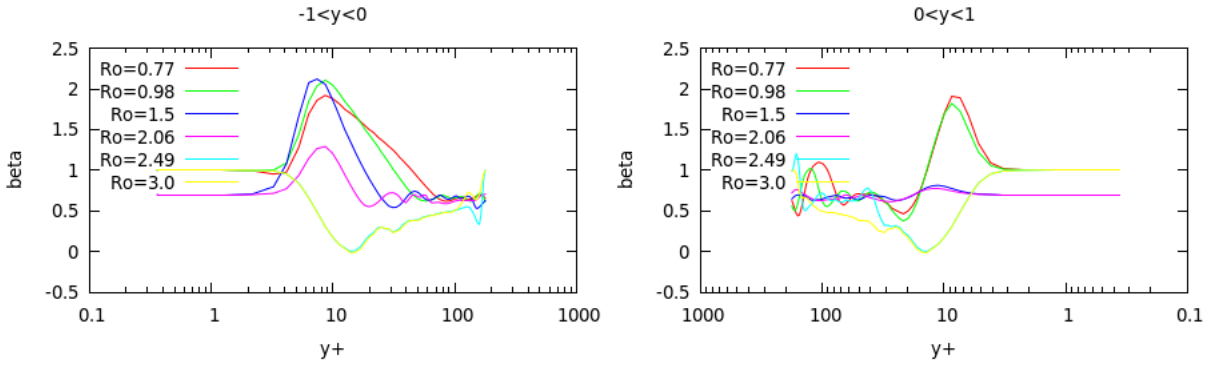

(a) β Profiles for k-production

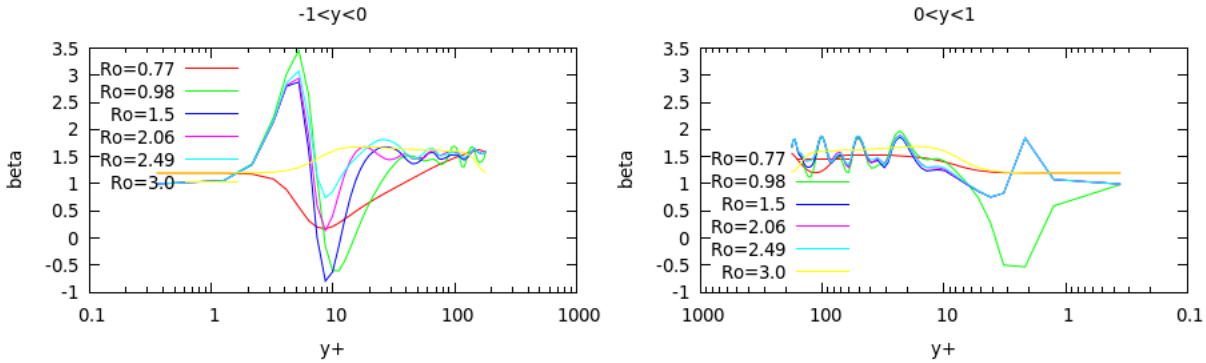

(b) β Profiles for k-dissipation

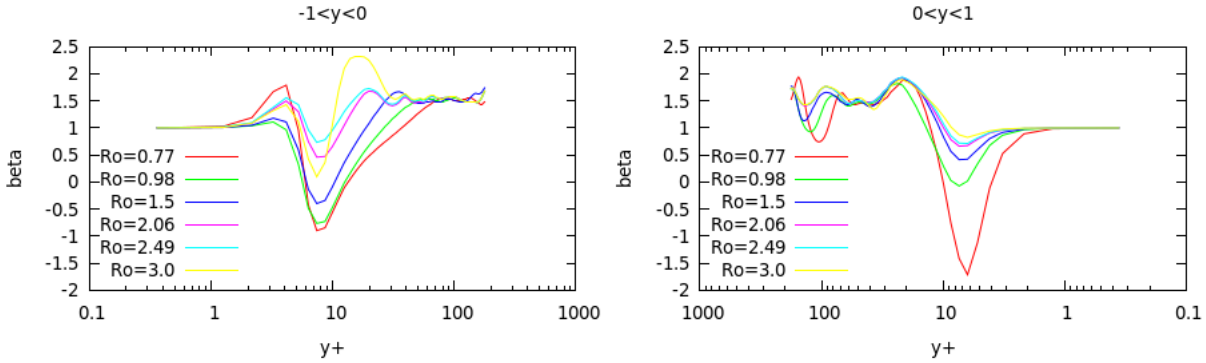

(c) β Profiles for ω-production

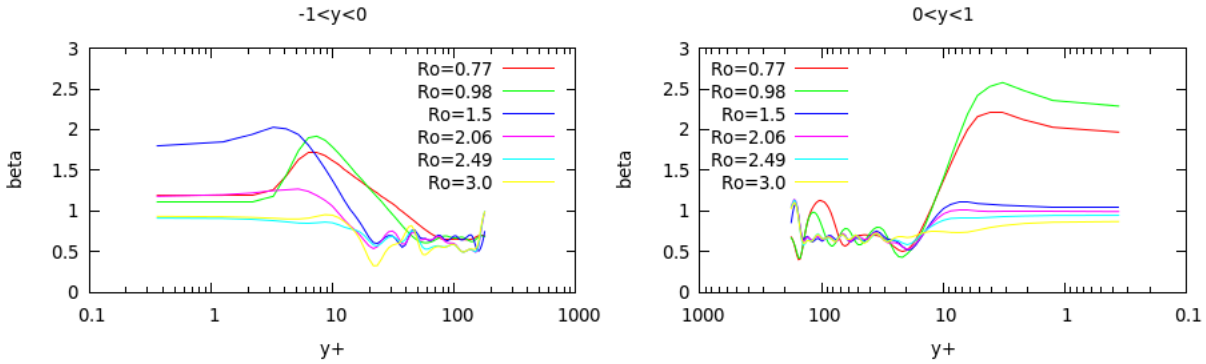

(d) β Profiles for ω-dissipation

Figure 4.13: β vs y+ for different terms

4.5 Future Scope

Application of the present work can be extended through the following studies as outlined by Parish and Duraisamy [27]:

- A detailed study to identify more scaling parameters. This step, on its own, might be advantageous in providing relevant *modeling* information for flows with spanwise rotation.
- Using machine learning strategies to *reconstruct* the missing fields of information, and
- *Injection* of these constructed parameters in k-ω model to enhance predicting capabilities.

CHAPTER 5. SUMMARY AND CONCLUSION

In this thesis, a formal methodology has been outlined for the inverse modeling of turbulent channel flow, both, with and without spanwise rotation. The main aim of this study has been to infer *functional* form of corrections for different terms in $k-\omega$ turbulence model. The inverse problem has been formally posed as an optimization problem and has been, then, solved using deterministic optimization methods. The usefulness of *adjoint* method, to find gradient of the *cost* function when *design* variable is high dimensional, has been discussed in detail. The formalism adopted here to get to the final equations has been based on *continuous* adjoint method and has been outlined in chapter II.

The results along with the usefulness and limitations of using such a strategy to inform closure modeling has been discussed in chapter IV of this thesis. For rotating channel flow case, β has been tried with various different terms of k-ω transport equations and has been found to yield good inverse results. Different *local minimums* have been found to exist almost in all cases and the *preference* of a particular results has been found to depend mainly on the choice of *prior* distribution of β. The *un-physical* nature of inverse results remains a problem that has to be addressed properly.

The ultimate goal of carrying out this inverse study is to identify non-dimensional parameters that can scale the correction terms. Towards this end, $\beta(y)$ for non-rotating case have been identified to scale with parameters like normalized wall distance, y^+ and turbulent Reynolds number, Re_T in the inner layer. However, unlike the non-rotating case, the scaling parameters for rotating case are not so easy to deduce. Below the laminar limit, rotating channel flow case has been found to scale somewhat with y^+. Future work entails a more through identification and study of different such parameters.

APPENDIX A. "FROZEN" VISCOSITY ADJOINT EQUATIONS

The Adjoint equations with "frozen" viscosity assumption can be derived following the same methodology outlined in chapter 2. They are simply outlined below:

$$\frac{\partial}{\partial y}\left[\left(\nu+\nu_t\right)\frac{\partial\lambda_1}{\partial y}\right]-\frac{\partial}{\partial y}\left[\left(2\beta\nu_t\frac{\partial\bar{u}}{\partial y}\right)\lambda_2\right]-\frac{\partial}{\partial y}\left[\left(2\gamma\frac{\partial\bar{u}}{\partial y}\right)\lambda_3\right]=-\left(\bar{u}-u_D\right) \tag{A.1}$$

$$\left[-\frac{1}{\omega}\frac{\partial\bar{u}}{\partial y}\frac{\partial\lambda_1}{\partial y}\right]+\left[\frac{\partial}{\partial y}\left(\left(\nu+\sigma^*\nu_t\right)\frac{\partial\lambda_2}{\partial y}\right)-\alpha^*\omega\lambda_2\right]=0 \tag{A.2}$$

$$\left[\frac{\nu_t}{\omega}\frac{\partial\bar{u}}{\partial y}\frac{\partial\lambda_1}{\partial y}\right]+\left[-\alpha^*k\lambda_2\right]+\left[\frac{\partial}{\partial y}\left(\left(\nu+\nu_t\right)\frac{\partial\lambda_3}{\partial y}\right)-2\alpha\omega\lambda_3\right]=0 \tag{A.3}$$

APPENDIX B. TKE IN OBJECTIVE FUNCTION DEFINITION

As already mentioned, any efforts to include TKE in objective function definition results in a wrong mean velocity profile. The results of one such effort with

$$F = \sum_{i=1}^{n} (k_i - k_{DNS_i})^2 \tag{B.1}$$

is shown in figure B.1. The inversion works well to match the TKE profiles (figure B.1a) but this results in an under-prediction of mean velocity profile (figure B.1b).

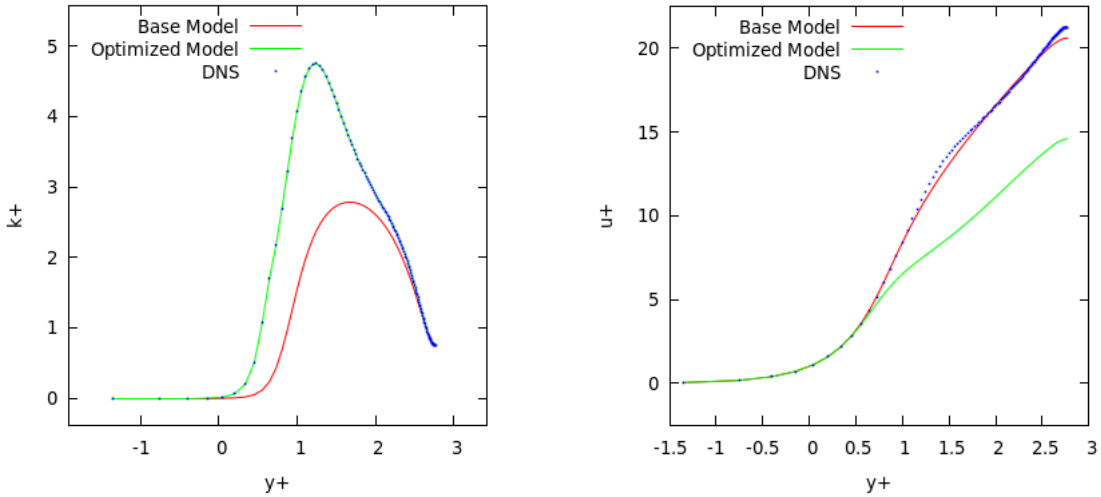

(a) TKE profile

(b) Mean velocity profile

Figure B.1: Inversion results when $F = \sum_{i=1}^{n} (k_i - k_{DNS_i})^2$ (for *non*-rotating channel flow with $Re_\tau = 590$)

APPENDIX C. CONVERGENCE PLOTS

Figure C.1 shows the rate of convergence of the optimization solver for cases with different rotation rates.

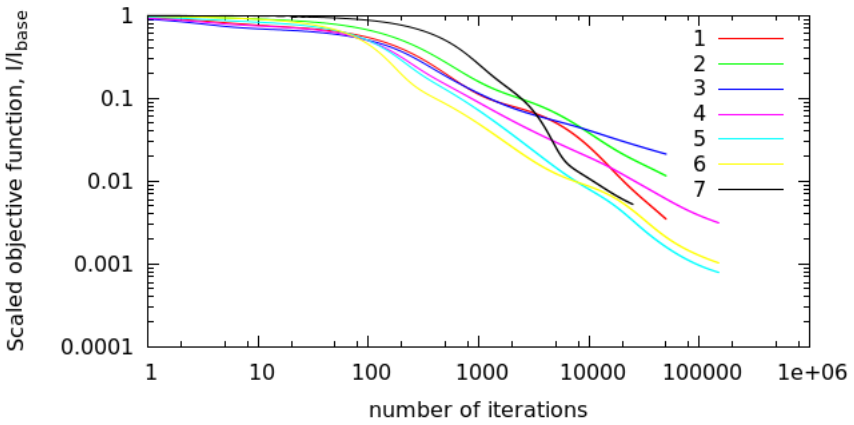

Figure C.1: Optimization convergence (with β in P_k) plots for rotating channel flow. I_{base} is the value of objective function when original k-ω model is used (i.e. when $\beta = 1$). Labels 1-7 represent the following rotation rates (in brackets): 1(0.00), 2(0.01), 3(0.05), 4(0.1), 5(0.15), 6(0.2) & 7(0.5)

Bibliography

[1] Dale Arden Anderson, John C Tannehill, and Richard H Pletcher. Computational fluid mechanics and heat transfer. 1984.

[2] S.K. Arolla. *Modeling and eddy simulation of rotating and curved turbulent fows.* PhD thesis, Iowa State University, 2013.

[3] Sunil K Arolla and Paul A Durbin. Modeling rotation and curvature effects within scalar eddy viscosity model framework. *International Journal of Heat and Fluid Flow*, 39:78–89, 2013.

[4] Jasbir Arora. *Introduction to optimum design.* Academic Press, 2004.

[5] Sai Hung Cheung, Todd A Oliver, Ernesto E Prudencio, Serge Prudhomme, and Robert D Moser. Bayesian uncertainty analysis with applications to turbulence modeling. *Reliability Engineering & System Safety*, 96(9):1137–1149, 2011.

[6] Lars Davidson. *An introduction to turbulence models.* 2001.

[7] Peter Alan Davidson. *Turbulence: an introduction for scientists and engineers.* Oxford University Press, 2015.

[8] Eric Dow and Qiqi Wang. Quantification of structural uncertainties in the k- ω turbulence model. *AIAA Paper*, 1762:2011, 2011.

[9] Karthikeyan Duraisamy, Ze Jia Zhang, and Anand Pratap Singh. New approaches in turbulence and transition modeling using data-driven techniques. *AIAA Paper*, 1284: 2015, 2015.

[10] Paul Durbin. Review: adapting scalar turbulence closure models for rotation and curvature. *Journal of Fluids Engineering*, 133(6):061205, 2011.

[11] Paul A Durbin and BA Pettersson Reif. *Statistical theory and modeling for turbulent flows*. John Wiley & Sons, 2011.

[12] Robert Ecke. The turbulence problem. *Los Alamos Science*, 29:124–141, 2005.

[13] Thomas D Economon, Francisco Palacios, and Juan J Alonso. A viscous continuous adjoint approach for the design of rotating engineering applications. *AIAA Paper*, 2580: 24–27, 2013.

[14] Heinz Werner Engl, Martin Hanke, and Andreas Neubauer. *Regularization of inverse problems*, volume 375. Springer Science & Business Media, 1996.

[15] G.L. Eyink. Turbulence notes, 2013. URL http://www.ams.jhu.edu/~eyink/Turbulence/.

[16] Michael B Giles and Niles A Pierce. An introduction to the adjoint approach to design. *Flow, turbulence and combustion*, 65(3-4):393–415, 2000.

[17] Olof Grundestam, Stefan Wallin, and Arne V Johansson. Direct numerical simulations of rotating turbulent channel flow. *Journal of Fluid Mechanics*, 598:177–199, 2008.

[18] A Hellsten. Some improvements to menter's k-ω sst turbulence model. *American Institute of Aeronautics and Astronautics*, 1998.

[19] Antony Jameson. Aerodynamic design via control theory. *Journal of scientific computing*, 3(3):233–260, 1988.

[20] Antony Jameson. Aerodynamic shape optimization using the adjoint method. *Lectures at the Von Karman Institute, Brussels*, 2003.

[21] Antony Jameson, L Martinelli, and NA Pierce. Optimum aerodynamic design using the navier–stokes equations. *Theoretical and computational fluid dynamics*, 10(1-4):213–237, 1998.

[22] S.G. Johnson. Notes on adjoint method, 2012. URL http://math.mit.edu/~stevenj/.

[23] Reidar Kristoffersen and Helge I Andersson. Direct simulations of low-reynolds-number turbulent flow in a rotating channel. *Journal of fluid mechanics*, 256:163–197, 1993.

[24] Robert D Moser, John Kim, and Nagi N Mansour. Direct numerical simulation of turbulent channel flow up to re_τ= 590. *Phys. Fluids*, 11(4):943–945, 1999.

[25] Todd A Oliver and Robert D Moser. Bayesian uncertainty quantification applied to rans turbulence models. In *Journal of Physics: Conference Series*, volume 318, page 042032. IOP Publishing, 2011.

[26] Eric Parish and Karthik Duraisamy. Quantification of turbulence modeling uncertainties using full field inversion. 2015.

[27] Eric J Parish and Karthik Duraisamy. A paradigm for data-driven predictive modeling using field inversion and machine learning. *Journal of Computational Physics*, 305:758–774, 2016.

[28] J Slotnick PI, A Khodadoust PM, J Alonso, D Darmofal, W Gropp, E Lurie, and D Mavriplis. Cfd vision 2030 study: a path to revolutionary computational aerosciences. 2013.

[29] Olivier Pironneau. On optimum design in fluid mechanics. *Journal of Fluid Mechanics*, 64(01):97–110, 1974.

[30] Stephen B Pope. *Turbulent flows*. IOP Publishing, 2001.

[31] Hassan Raiesi, Ugo Piomelli, and Andrew Pollard. Evaluation of turbulence models using direct numerical and large-eddy simulation data. *Journal of Fluids Engineering*, 133(2): 021203, 2011.

[32] Anand Pratap Singh and Karthik Duraisamy. Using field inversion to quantify functional errors in turbulence closures. *Physics of Fluids (1994-present)*, 28(4):045110, 2016.

[33] Pavel E Smirnov and Florian R Menter. Sensitization of the sst turbulence model to rotation and curvature by applying the spalart–shur correction term. *Journal of Turbomachinery*, 131(4):041010, 2009.

[34] PR Spalart and M Shur. On the sensitization of turbulence models to rotation and curvature. *Aerospace Science and Technology*, 1(5):297–302, 1997.

[35] T Taylor, Francisco Palacios, Karthik Duraisamy, and J Alonso. A hybrid adjoint approach applied to turbulent flow simulations. In *21st AIAA Computational Fluid Dynamics Conference, San Diego, June*, pages 24–27, 2013.

[36] Thomas William Richard Taylor. *A hybrid adjoint approach for systems of arbitrarily complex partial differential equations*. PhD thesis, Stanford University, 2013.

[37] Brendan Tracey, Karthik Duraisamy, and Juan J Alonso. A machine learning strategy to assist turbulence model development. *AIAA Paper*, 1287:2015, 2015.

[38] David C Wilcox et al. *Turbulence modeling for CFD*, volume 2. DCW industries La Canada, CA, 1998.

[39] ME Young and A Ooi. Comparative assessment of les and urans for flow over a cylinder at a reynolds number of 3900. In *16th Australasian Fluid Mechanics Conference (AFMC)*, pages 1063–1070. School of Engineering, The University of Queensland, 2007.

[40] Ze Jia Zhang and Karthikeyan Duraisamy. Machine learning methods for data-driven turbulence modeling. *AIAA*, 2460:2015, 2015.

[41] AS Zymaris, DI Papadimitriou, KC Giannakoglou, and C Othmer. Continuous adjoint approach to the spalart–allmaras turbulence model for incompressible flows. *Computers & Fluids*, 38(8):1528–1538, 2009.